

LA-9468-PR

Progress Report

CIC-14 REPORT COLLECTION

REPRODUCTION  
COPY



Los Alamos National Laboratory is operated by the University of California for the United States Department of Energy under contract W-7405-ENG-36.

*Applied Nuclear Data  
Research and Development*

*October 1, 1981—March 31, 1982*

LOS ALAMOS NATIONAL LABORATORY  
3 9338 00308 1717

**Los Alamos** Los Alamos National Laboratory  
Los Alamos, New Mexico 87545

The four most recent reports in this series, unclassified, are LA-8757-PR, LA-8874-PR, LA-9060-PR and LA-9262-PR.

This work was performed under the auspices of the US Department of Energy's Division of Reactor Research and Technology, Office of Basic Energy Sciences, and Office of Fusion Energy; the Spent Fuel Project Office under the technical direction of the Savannah River Laboratory; the Electric Power Research Institute; and the Nuclear Regulatory Commission.

DISCLAIMER

This report was prepared as an account of work sponsored by an agency of the United States Government. Neither the United States Government nor any agency thereof, nor any of their employees, makes any warranty, express or implied, or assumes any legal liability or responsibility for the accuracy, completeness, or usefulness of any information, apparatus, product, or process disclosed, or represents that its use would not infringe privately owned rights. References herein to any specific commercial product, process, or service by trade name, trademark, manufacturer, or otherwise, does not necessarily constitute or imply its endorsement, recommendation, or favoring by the United States Government or any agency thereof. The views and opinions of authors expressed herein do not necessarily state or reflect those of the United States Government or any agency thereof.

LA-9468-PR  
Progress Report

UC-34c  
Issued: August 1982

# Applied Nuclear Data Research and Development

October 1, 1981—March 31, 1982

Compiled by  
P. G. Young



**Los Alamos** Los Alamos National Laboratory  
Los Alamos, New Mexico 87545

## CONTENTS

I.	THEORY AND EVALUATION OF NUCLEAR CROSS SECTIONS.....	1
A.	Peripheral Effects in R-Matrix Theory.....	1
B.	Charged-Particle Elastic Cross Sections.....	2
C.	Energy-Angle Correlated Emission Spectra from the D(n,2n)P Reaction.....	4
D.	New ENDF/B-V Evaluation of n+ <sup>7</sup> Li Reactions.....	6
E.	Calculation of Proton Emission Spectra from p+ <sup>91</sup> Zr and p+ <sup>87</sup> Sr Reactions.....	10
F.	Thulium Cross-Section Calculations.....	10
G.	Production of a New Evaluation for Natural Tungsten between 0.1 and 20 MeV.....	13
H.	Application and Further Development of the Improved COMNUC Fission Model.....	25
I.	Inelastic Cross-Section Calculations on <sup>239</sup> Pu.....	28
J.	New Calculation of Prompt Fission Neutron Spectrum N(E) and Average Prompt Neutron Multiplicity $\bar{\nu}_p$ .....	31
K.	New Fission Neutron Spectrum Representation for ENDF.....	31
L.	Calculation of the Prompt Neutron Spectrum and Average Prompt Neutron Multiplicity for the Spontaneous Fission of <sup>252</sup> Cf.....	31
M.	Calculation of Excited-State Cross Sections for Actinide Nuclei.....	32
II.	NUCLEAR CROSS-SECTION PROCESSING AND TESTING.....	33
A.	NJOY Code Development.....	33
B.	New 80-Group Fast Reactor Cross-Section Library.....	35
C.	NJOY Covariance Modules, ERRORR and COVR.....	39
D.	Integral Data Testing of Representations of <sup>235</sup> U and <sup>239</sup> Pu Thermal Fission Spectra.....	47
III.	FISSION PRODUCTS AND ACTINIDES: YIELDS, DECAY DATA, DEPLETION, AND BUILDUP.....	57
A.	ENDF/B-VI Yields.....	57
B.	Delayed Neutron Data.....	57
C.	CRAY Code Conversions.....	72
D.	Calculating Fission-Product Decay-Energies and Spectra Using Adjusted Data.....	72
E.	Calculated Neutron Sources in Pu Process Solutions.....	75
REFERENCES.....		80

APPLIED NUCLEAR DATA RESEARCH AND DEVELOPMENT  
SEMIANNUAL PROGRESS REPORT  
October 1, 1981 - March 31, 1982

Compiled by

P. G. Young

ABSTRACT

This progress report describes the activities of the Los Alamos Nuclear Data Group for October 1, 1981, through March 31, 1982. The topical content is summarized in the Table of Contents.

---

I. THEORY AND EVALUATION OF NUCLEAR CROSS SECTIONS

A. Peripheral Effects in R-Matrix Theory (G. M. Hale)

The spinless, one-dimensional treatment of peripheral effects in R-matrix theory described in a previous report<sup>1</sup> has been generalized to the case of three dimensions and finite-mass transferred particles, including spin. As they do in the one-dimensional case, peripheral overlap effects in this case lead to "particle-exchange" poles in the R matrix for proper choice of the boundary conditions, which have the form

$$R_{12}^x = R_{21}^x = \frac{-(-1)^\ell C_1 C_2 d_s W_\ell(a_1, a_2)}{\epsilon_x - \epsilon} .$$

Here  $W_\ell$  is a projection of the overlapping bound states on the channel surface that acts as a sort of  $\ell$ -dependent "width" for particle exchange;  $d_s$  is a spin-function overlap factor;  $C_1$  and  $C_2$  are dimensionless normalization constants

for the asymptotic tails of the bound-state wavefunctions; and  $\varepsilon_x$  is the position of the pole, which is always negative, and depends only on the binding energies and masses of the particles.

The type of term described above is unconventional in R-matrix theory for two reasons. In a reaction, it contributes only to the off-diagonal elements of the R matrix, whereas the usual resonance poles that contribute to a reaction necessarily have non-zero diagonal elements. For elastic scattering, due to the  $(-1)^\ell$  factor that is characteristic of particle exchange, the residues of the pole alternate sign with  $\ell$ , whereas the residues of conventional resonance poles all have the same sign for elastic scattering. These characteristics can give, in general, a different behavior of the collision matrix from that obtainable from conventional R-matrix theory, while preserving its properties of unitarity and symmetry. One result, for instance, would be more pronounced backward peaking in elastic differential cross sections at low energies than can be obtained from the conventional theory at a given radius.

We are currently applying the revised theory including peripheral effects to an analysis of reactions in the  ${}^7\text{Li}$  system. The contribution of the deuteron exchange pole to the  ${}^6\text{Li}(n,t)$  reaction appears to account for a significant amount of  $1/v$  cross section at low energies. We plan next to consider the effects of the deuteron exchange pole on  $p$ - ${}^3\text{He}$  and  $n$ -T elastic scattering where it may provide the increased backward peaking needed to describe adequately precise measurements of the  $p$ - ${}^3\text{He}$  differential cross section at low energies, and possibly explain the rather poorly understood behavior of the s-waves for  $n$ -T scattering at low energies.

B. Charged-Particle Elastic Cross Sections [G. M. Hale, D. C. Dodder, and J. C. De Veaux (U. Illinois)]

The slowing down of charged particles in a plasma has, in the past, concerned particles with energies sufficiently low to assume that the dominant mechanism is Coulomb elastic scattering. However, current fusion studies are sometimes concerned with the slowing down of fast ions, in which the nuclear components of the scattering are important at large angles, and enter even at small angles through interference with the Coulomb amplitude. Using a format developed at Los Alamos that allows an exact Legendre polynomial representation of  $\sigma_{NI}(\mu)$ , the difference of the elastic scattering cross section and the Rutherford (or "pure Coulomb") cross section at  $\mu = \cos \theta_{CM}$ , we are constructing

a file of elastic cross sections for most of the possible interactions between light ions from protons through alpha particles, at energies up through several MeV.

The cross sections are calculated from parameters obtained over the years from the extensive Los Alamos program of R-matrix analyses of light systems, and are generally based on large data bases that contain many other measurements in addition to elastic cross sections. R-matrix theory provides an explicit separation of nuclear and Coulomb effects in the cross section, and reasonable extrapolations to low energies, particularly in the presence of low-lying resonances, as in the case of d-T scattering.

Figure 1 shows the results of various integrals involving  $\sigma_{NI}(\mu)$  for d-T scattering, compared to evaluations at Livermore reported by Perkins and Cullen,<sup>2</sup>

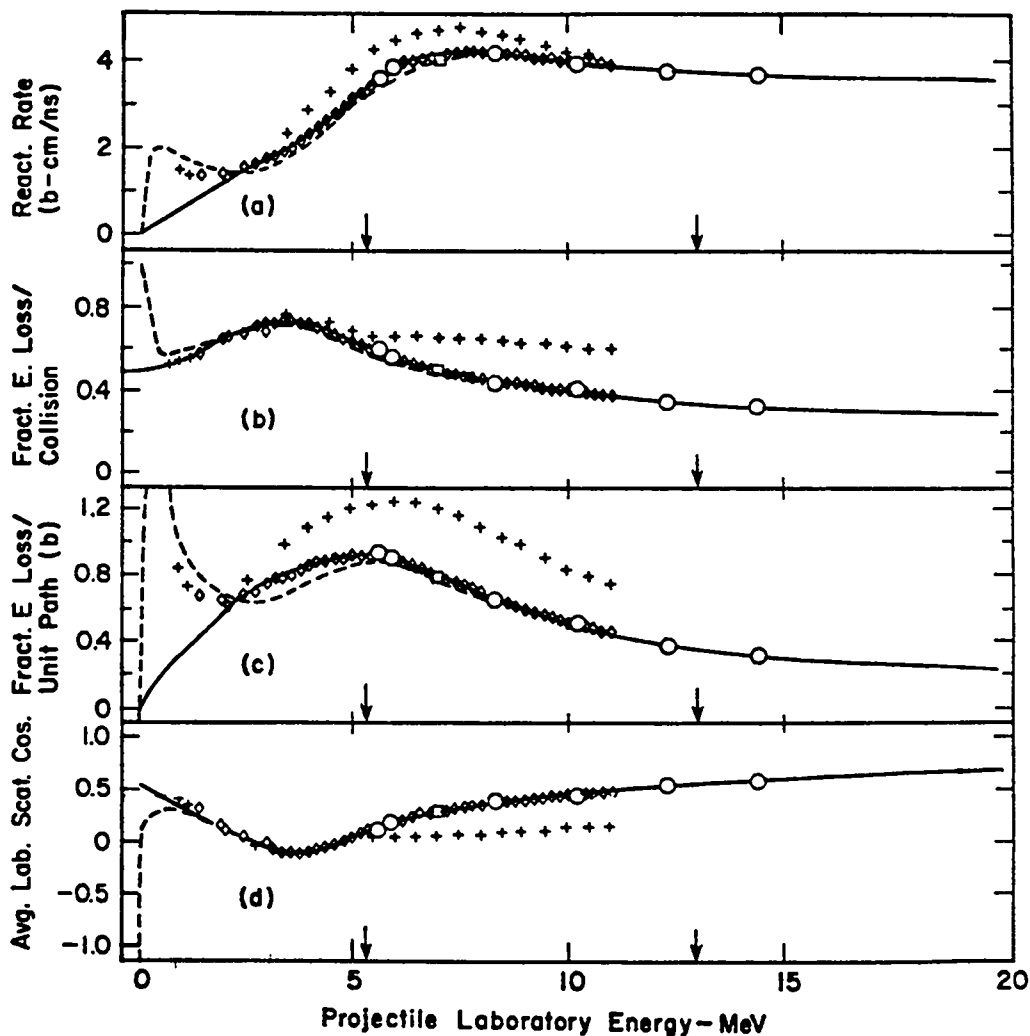


Fig. 1. Integrals of  $\sigma_{NI}(\mu)$  for d-T scattering. The solid curves are the evaluations of Perkins and Cullen; the dashed curves are calculated from Los Alamos cross sections; and the points represent experimental data.

The solid curves are the Livermore results and the dashed curves are the Los Alamos calculations. In both cases, the upper limits of the integrals over  $\mu$  are given by  $\min (.94, \mu_0)$ , where  $\sigma_{NI}(\mu_0) = 0$ , in order to define values of the integrals that correspond to positive integrated cross sections. The integral quantities are seen to disagree substantially in the region of the low-energy d-T resonance where the Livermore extrapolations to zero energy are somewhat oversimplified owing to the lack of elastic cross-section data.

C. Energy-Angle Correlated Emission Spectra from the D(n,2n)P Reaction (P. G. Young)

The existing ENDF/B-V evaluation for neutron reactions on deuterium uses a representation for the D(n,2n)P reaction that ignores the pronounced energy-angle correlations in the secondary neutron spectra. This limitation is caused by format and processing code restrictions on Version V of ENDF/B. In order to investigate possible effects in applied problems from errors in the emission spectra, a modified version of the ENDF/B-V evaluation has been developed that uses a simple model to specify energy-angle correlations in the (n,2n) neutron emission spectra.

Using a technique first employed<sup>3</sup> to represent energy-angle data from the  $^9\text{Be}(n,2n)$  reaction, the D(n,2n) reaction in the ENDF/B-V evaluation was recast into a special excitation-energy-bin format that uses the reaction designators MT = 51-87 to represent the data. In this formulation the MT = 4 cross section, which is the sum of MT = 51-87, actually represents the (n,2n) reaction. In computing an emission spectrum, however, each of the MT = 51-87 cross sections must be doubled because two neutrons are emitted per reaction. The NJOY processing code properly accounts for this effect, and the kinematic energy-angle correlations are automatically preserved in the processing because of the MT = 51-87 level representation.

The excitation-energy-bin representation was implemented using a simple 3-body phase space model to apportion the cross section among the MT = 51-87 reaction types. This model has been found to reasonably describe measured spectra from the D(n,2n) reaction and certainly approximates the kinematics of the reaction far better than does ENDF/B-V. Isotropic angular distributions were assumed in the center-of-mass system for each of the MT = 51-87 energy bins, and the sum of the reaction was normalized to the ENDF/B-V D(n,2n) cross section. All other data in the revised evaluation are taken from ENDF/B-V.

A comparison between neutron emission spectra calculated from the present work and ENDF/B-V is shown in Fig. 2 for an incident neutron energy of 15 MeV and for  $\theta_{\text{LAB}} = 0^\circ, 90^\circ, \text{ and } 180^\circ$ . The peak at higher energy in each spectrum is elastic scattering, and the lower energy distribution results from the (n,2n) reaction. The problem with the energy-angle uncorrelated representation for ENDF/B-V is evident in Fig. 2.

Included in Table I is a comparison of the average neutron emission energies for  $E_n = 5, 10, 15$  MeV and  $\theta_{\text{LAB}} = 0^\circ, 90^\circ, 180^\circ$ . Large differences between ENDF/B-V and the present work are evident, especially for the (n,2n) reaction but also for the total energy [elastic plus (n,2n)].

The new evaluation will be provided to the ENDF/A library at the National Nuclear Data Center in Brookhaven. The evaluation is being processed with the NJOY code<sup>4</sup> and will be made available in MATXS format at the National Magnetic Fusion Energy Computer Center at Livermore.

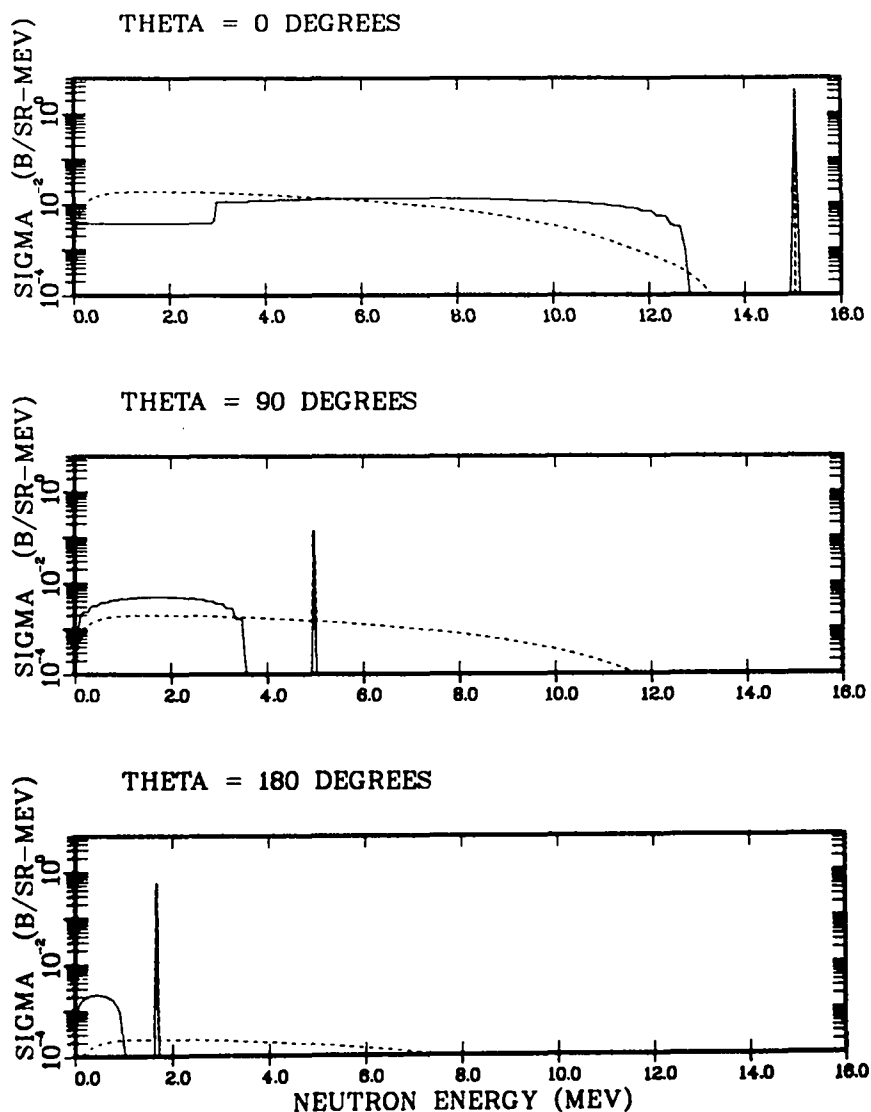


Fig. 2. Neutron emission spectra at 3 angles from the D(n,2n)P reaction with 15-MeV incident neutrons. The solid curve was calculated from the present evaluation and the dashed curve from ENDF/B-V.

TABLE I

COMPARISON OF AVERAGE SECONDARY NEUTRON ENERGIES FROM ENDF/B-V  
AND THE PRESENT EVALUATION FOR THE (n,2n) REACTION  
AND FOR THE TOTAL EMISSION SPECTRUM

$E_n$ (MeV)	$\theta$	ENDF/B-V		LA-82		$\Delta_{n,2n}$ (%)	$\Delta_{total}$ (%)
		$E_{n,2n}$ (MeV)	$E_{total}$ (MeV)	$E_{n,2n}$ (MeV)	$E_{total}$ (MeV)		
5	0°	0.955	4.684	1.301	4.716	36.2	0.7
	90°	0.955	1.673	0.092	1.662	-90.3	-0.7
	180°	0.0	0.575	0.025	0.575	—	0
10	0°	2.613	8.493	4.116	8.858	57.5	4.3
	90°	2.613	3.087	0.931	2.520	-64.4	-18.4
	180°	2.613	1.146	0.219	1.100	-91.6	-4.0
15	0°	4.273	11.863	6.895	12.739	61.4	7.4
	90°	4.273	4.509	1.760	2.839	-58.8	-37.0
	180°	4.273	1.819	0.477	1.606	-88.8	-11.7

D. New ENDF/B-V Evaluation of  $n+{}^7\text{Li}$  Reactions (P. G. Young)

A new evaluation of neutron-induced reactions on  ${}^7\text{Li}$  has been completed and submitted to the National Nuclear Data Center at Brookhaven for Revision 2 of the ENDF/B-V evaluated data library. The new evaluation includes a variance-covariance analysis of the major reaction cross sections, a complete reanalysis of all elastic and inelastic angular distribution data, a division of the (n,nt) cross section into a series of excitation energy bins that permit inclusion of accurate energy-angle correlations for emission neutrons, and complete covariance files for all cross-section data and (n,nt) neutron emission spectra.

The variance-covariance analysis has been described previously<sup>5,6</sup> and will not be detailed here. Basically, the analysis utilized the GLUCS code system, developed at Oak Ridge National Laboratory,<sup>7</sup> to perform variance-covariance analyses of each of the major cross-section types for which experimental data exist. The results of this analysis were then combined using the Los Alamos code ALVIN<sup>8</sup> under the constraint that all partial reactions sum to the total cross section, with full account being taken of all covariances.

The evaluated elastic and inelastic neutron angular distributions were obtained from a Legendre coefficient analysis of all the available experimental data. The experiments of Lane et al.,<sup>9</sup> Knitter and Coppola,<sup>10</sup> Knox et al.,<sup>11</sup> Knox and Lane,<sup>12</sup> and Hogue et al.<sup>13</sup> were emphasized in the elastic angular distribution evaluation. Figure 3 compares the measurements of Hogue et al. at 4 energies to the new evaluation. Because there are no elastic angular distribution data above 14.1 MeV, a spherical optical model calculation was used to extrapolate the angular distributions to 20 MeV. The resulting parameters are given in Ref. 5.

Because the customary representations used for ENDF/B evaluations do not permit inclusion of energy-angle correlation effects in secondary neutron emission data from (n,xn) reactions, we used an excitation-energy binning technique to represent the  ${}^7\text{Li}(n,nt)$  reaction. With this technique the continuum neutrons from (n,nt) reactions are described as a series of lumped, discrete scattering levels, each representing a bin of excitation energy in the residual nucleus and each with a separate energy-dependent cross section and angular distribution. When these data are processed into multigroup form, the kinematic energy-angle correlations are automatically preserved.

The evaluation of the (n,nt) data into excitation energy bins was based upon the neutron emission spectrum measurements of Lisowski et al.<sup>14</sup> using monoenergetic neutrons from the Los Alamos Tandem Van de Graaff at 6, 10, and 14 MeV. The results are compared in Fig. 4 to the spectra measured at the Oak Ridge Electron Linear Accelerator (ORELA) by Morgan<sup>15</sup> at 55° and 125° for an incident neutron energy bin of 12.45-14.95 ( $\bar{E} = 13.7$ ) MeV. The broad peaks at higher energy are from elastic scattering, and the lower energy spectra result from the (n,nt) reaction.

Complete covariance files for the major cross-section types and for the excitation energy bins are included in the evaluation. The latter data determine the correlated errors in the neutron emission spectra from the (n,nt) reaction. Covariances for the cross sections were taken directly from the GLUCS-ALVIN analysis, when possible, and are based on those results for all major reaction types. The errors and cross correlations for the emission spectra were estimated from the Lisowski<sup>14</sup> experimental errors, but the final results were adjusted via the ALVIN code to be consistent with results from the independent GLUCS-ALVIN cross-section analysis.

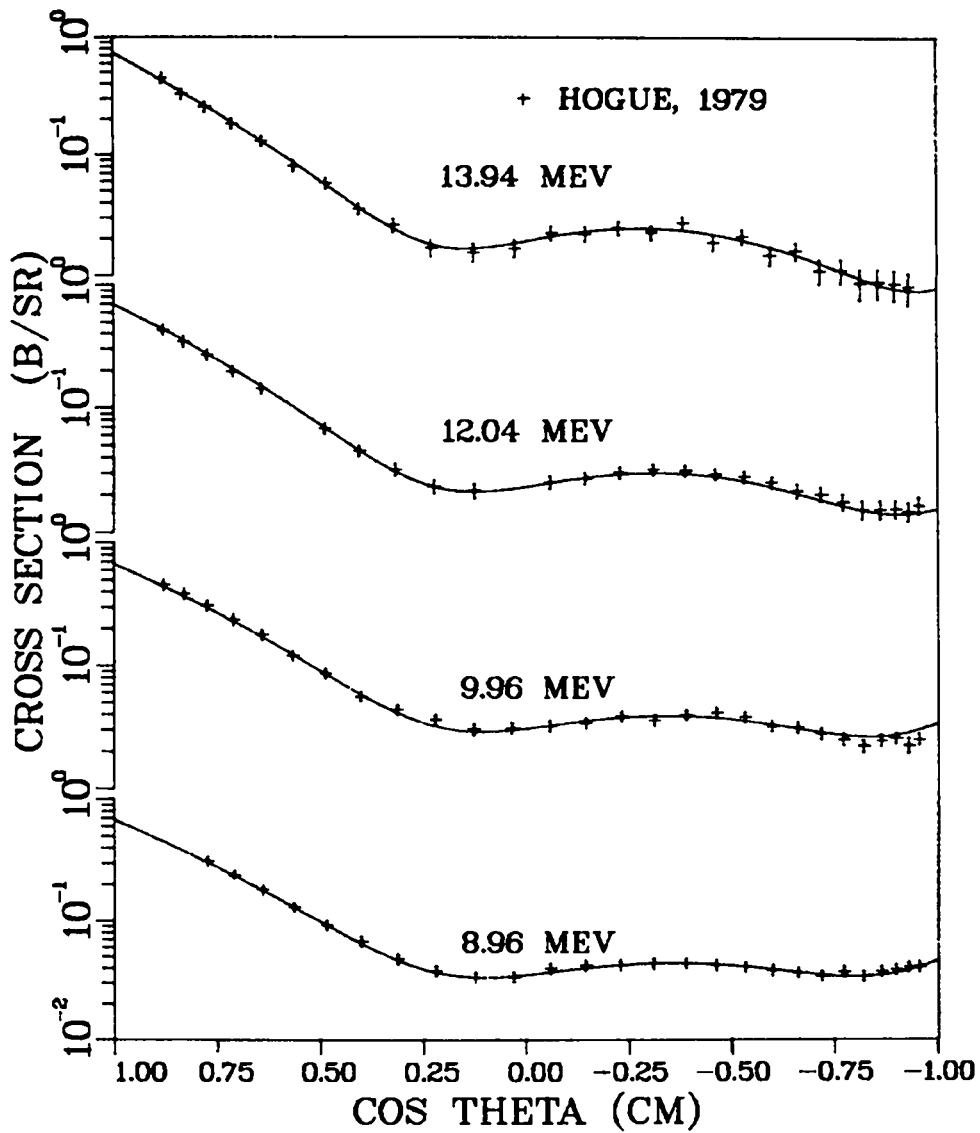
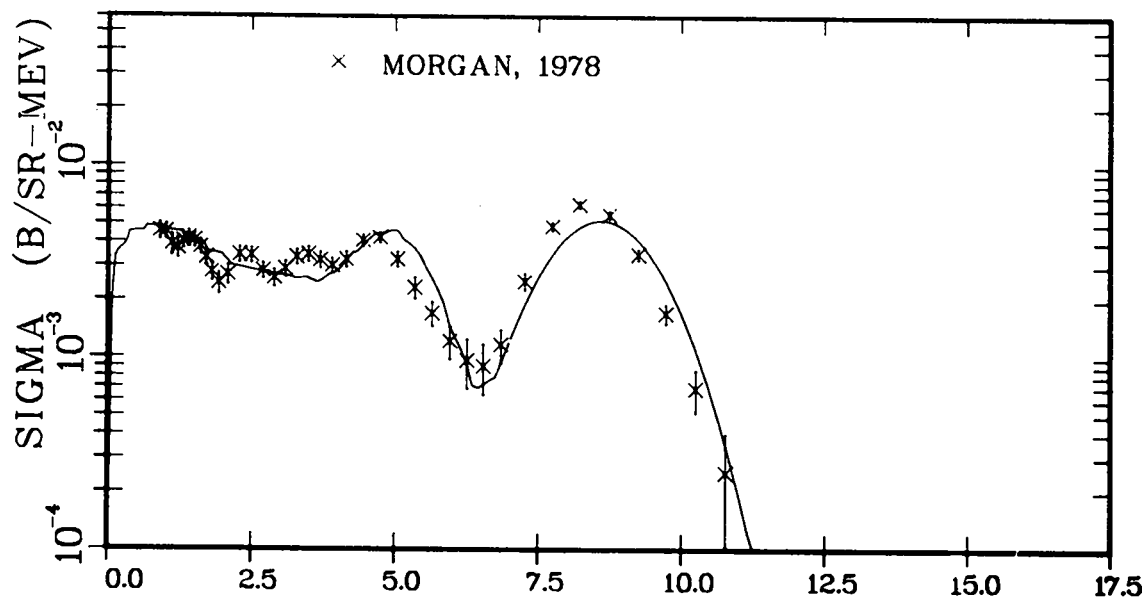


Fig. 3. Comparison of the  $n+{}^7\text{Li}$  elastic angular distribution measurement by Hogue et al.<sup>13</sup> to the present evaluation. Both measurement and evaluation include the  ${}^7\text{Li}(n,n')$  reaction to the first excited state of  ${}^7\text{Li}$ .

THETA = 126 DEGREES



THETA = 50 DEGREES

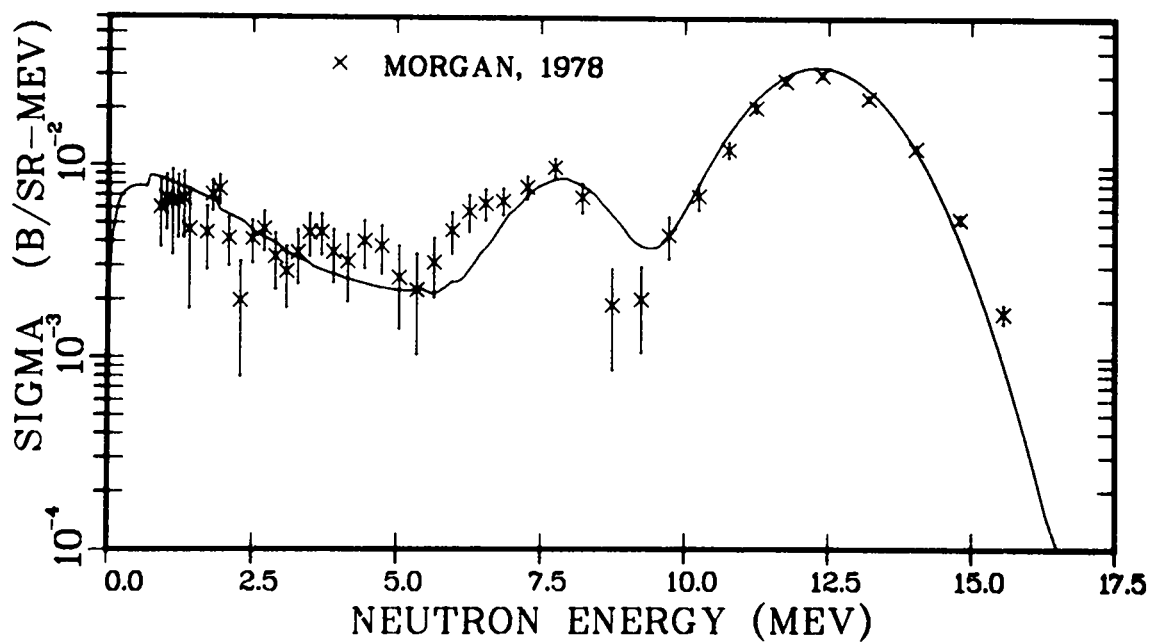


Fig. 4. Measured and evaluated neutron emission spectra from  $n+{}^7\text{Li}$  reactions with 13.7-MeV incident neutrons.

E. Calculation of Proton Emission Spectra from  $p+^{91}\text{Zr}$  and  $p+^{87}\text{Sr}$  Reactions  
(E. D. Arthur)

Recently, experimental measurements have begun at the Los Alamos Tandem Van de Graaff of the proton emission spectra from  $p+^{91}\text{Zr}$  and  $p+^{87}\text{Sr}$  reactions for proton energies between 12 and 18 MeV. Reactions on these nuclei produce compound systems having large "proton windows" resulting from proton binding energies that are appreciably less than those for neutrons. Such measurements, particularly for the  $p+^{87}\text{Sr}$  system, can provide information relevant to our theoretical analysis of  $n+^{87}\text{Y}$  reactions, especially for those reactions involving low-energy proton emission.

Because of target contaminant problems for  $^{87}\text{Sr}$ , it is not possible to measure directly the low-energy protons from (p,np) and (p,pn) reactions that are of interest for our nuclear model calculations. Instead, these protons must be detected in coincidence with a neutron, which introduces complications in the analysis of such data resulting from neutron detector threshold and efficiency effects. In order to compare directly to such data, we have modified the code<sup>16</sup> that disentangles particle emission spectra produced in our nuclear model calculations using the GNASH preequilibrium Hauser-Feshbach code. We are now able to calculate the proton emission spectrum in "coincidence" with neutron emission, while including a mockup of the neutron detector characteristics in the formulation of the "coincidence" requirement. Figure 5 illustrates our calculated emission spectrum for low-energy protons resulting from (p,np) and (p,pn) reactions induced by 16-MeV protons on  $^{91}\text{Zr}$ . The solid curve includes no neutron detector effects, while the dashed curve includes a threshold and efficiency similar to that used in the experimental measurements. Such detector effects prevent the detection of higher energy protons associated with the emission of a low-energy neutron. They also distort significantly the proton emission spectrum resulting from the (p,pn) reaction. Overall inclusion of these effects produces a qualitative shape agreement to preliminary proton emission spectra from this experiment that would be lacking otherwise.

F. Thulium Cross-Section Calculations (E. D. Arthur)

We have noted that the low-energy reaction cross sections obtained from our coupled-channel calculations<sup>17</sup> on  $^{169}\text{Tm}$  do not agree with results obtained from optical model calculations using the Moldauer<sup>18</sup> optical model set. Even though the Moldauer parameters are spherical ones, they were obtained from fits to low-energy neutron data and generally reproduce quite successfully

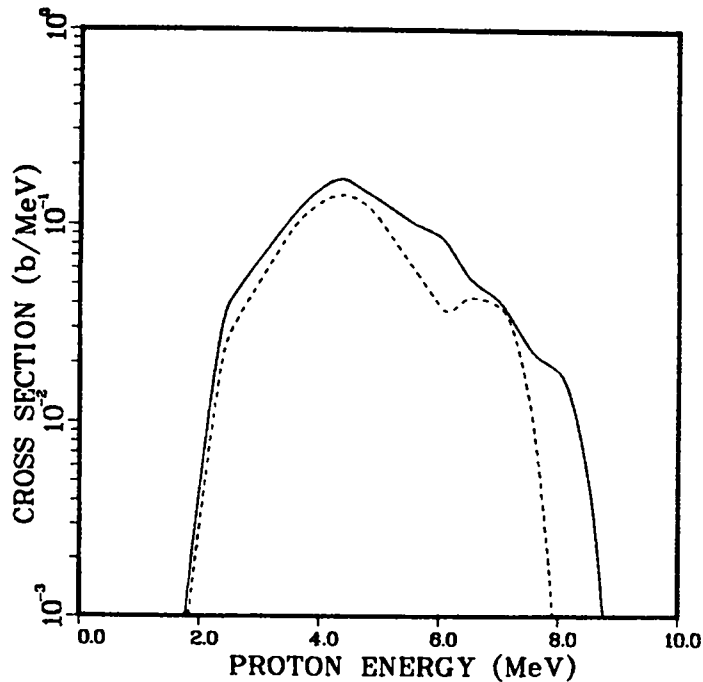


Fig. 5. Comparison of calculated proton emission spectra resulting from 16-MeV proton reactions on  $^{91}\text{Zr}$ . The comparison is restricted to protons associated with neutron emission [sum of (p,np) and (p,pn) contributions]. The dashed and solid curves illustrate spectra calculated with and without inclusion of neutron detector effects.

total cross sections, s- and p-wave strengths, and potential scattering radii for energies below a few MeV. In Fig. 6 we compare nonelastic cross sections obtained from these two parameter sets. Similar comparisons are made in Fig. 7 for the  $^{165}\text{Ho}$  total cross section, where the coupled-channel parameters used in our  $n + ^{169}\text{Tm}$  calculations<sup>17</sup> produce much better agreement to the experimental data. Comparisons to s- and p-wave strength data for  $^{165}\text{Ho}$  and  $^{169}\text{Tm}$  yield similar results. Our conclusions are that, even though the Moldauer optical parameters produce good agreement to data for nuclei up to  $A = 140$ , they are not adequate for use with permanently deformed nuclei in this region of the periodic table.

To further test the nuclear models and their parameters, experimental measurements<sup>19</sup> have been made recently of the 14-MeV (n,2n) cross section on the unstable  $^{168}\text{Tm}$  isotope. Our calculations are compared to preliminary results from this experiment in Fig. 8. The good agreement indicates that our parameters work well for this nucleus and show, indirectly, that the total direct-reaction component of the inelastic scattering cross section is comparable to that for  $^{169}\text{Tm}$ , even though a well-defined rotational structure does not exist for  $^{168}\text{Tm}$ .

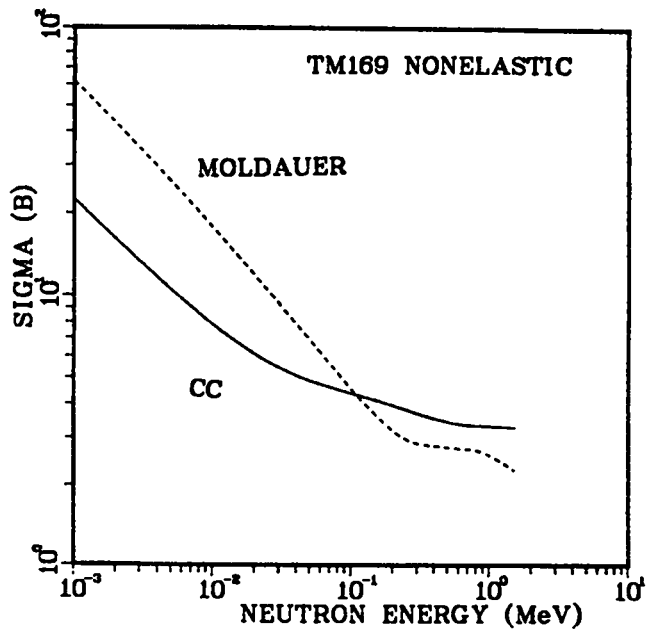


Fig. 6. A comparison of  $n+^{169}\text{Tm}$  non-elastic cross sections obtained using the coupled-channel optical parameters of Ref. 18 (solid curve) and the Moldauer optical model set.

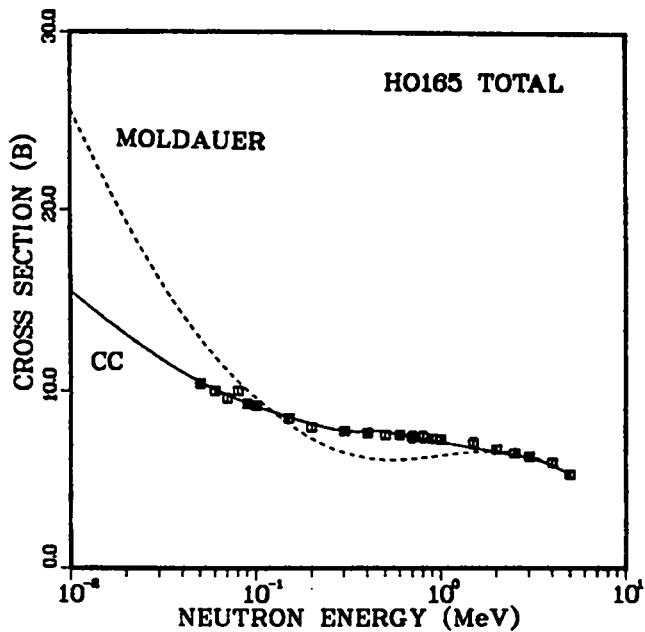


Fig. 7. A similar comparison as that for Fig. 6 to total cross-section data available for  $^{165}\text{Ho}$ .

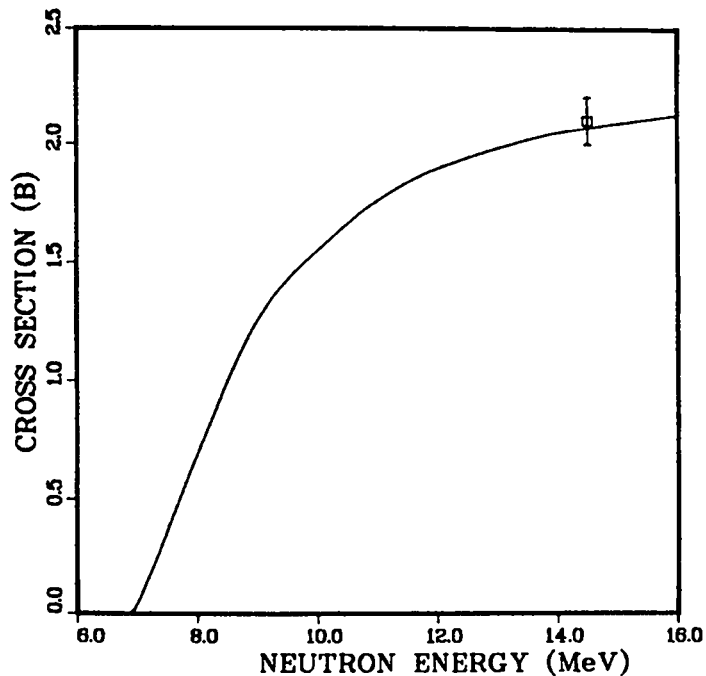


Fig. 8. The calculated  $^{168}\text{Tm}(n,2n)$  cross section is compared to preliminary experimental data for this reaction at 14 MeV.

G. Production of a New Evaluation for Natural Tungsten between 0.1 and 20 MeV (E. D. Arthur and P. G. Young)

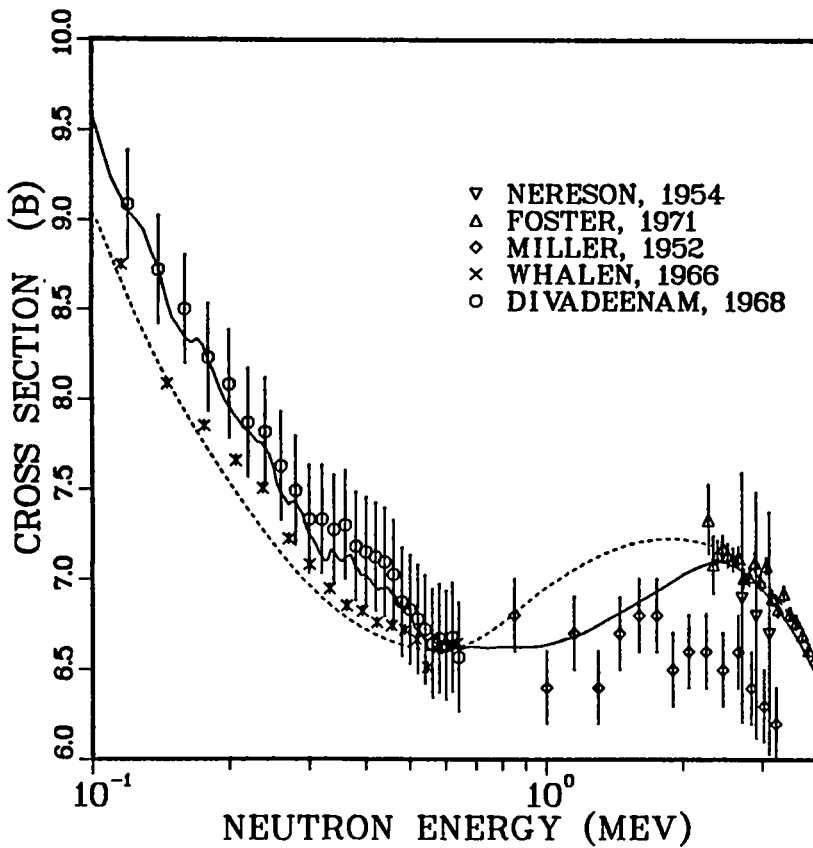
An evaluated data file for neutron reactions on natural tungsten between 0.1 and 20 MeV has been made through combination of new evaluations for the  $^{182,183,184,186}\text{W}$  isotopes completed recently.<sup>20,21</sup> The resultant file has been checked through numerous comparisons to experimental data and through use of ENDF checking codes available from Brookhaven National Laboratory.

Since the elemental tungsten evaluated data file was constructed through use of the isotopic evaluations, which were in turn based on extensive model calculations, a direct link may not always exist between this new natural evaluation and data measured for natural tungsten. We have instead relied on the quality and consistency of the isotopic experimental data along with constraints introduced through our application of the relevant nuclear models. The success of this technique is illustrated through comparison of the evaluation to experimental data available for the major reaction channels of natural tungsten.

Figure 9 compares our evaluated total cross section (solid curve) to experimental data and to the ENDF-B/V evaluation (dashed curve). A similar comparison is shown in Fig. 10 for the elastic cross section. Numerous experimental measurements have been made of neutrons elastically scattered from natural tungsten, but some of the more recent and complete sets of such measurements are those of Kinney.<sup>22</sup> We compare to these angular distributions in Fig. 11. Within these comparisons there is general agreement between our evaluation and experimental total and elastic cross-section data. Such agreement, along with isotopic data, implies realistic values for the total reaction cross section. Since (n,xn) cross sections are a major constituent of the total reaction cross section, we compare the evaluated cross sections in Fig. 12 to recent data available for (n,2n) and (n,3n) reactions from threshold to 20 MeV. Again, reasonable agreement is obtained.

A major deficiency of the ENDF/B-V evaluation was the significant underprediction of portions of the neutron emission spectrum caused by failure to consider the influence of preequilibrium processes at incident energies above 10 MeV. In the present evaluation this deficiency has been rectified as shown in Fig. 13, where the evaluated spectrum is compared to several neutron emission measurements performed around 14 MeV. The agreement is good particularly with the precise data recently measured by Vonach.<sup>23</sup>

### W-NAT TOTAL CROSS SECTION



### W-NAT TOTAL CROSS SECTION

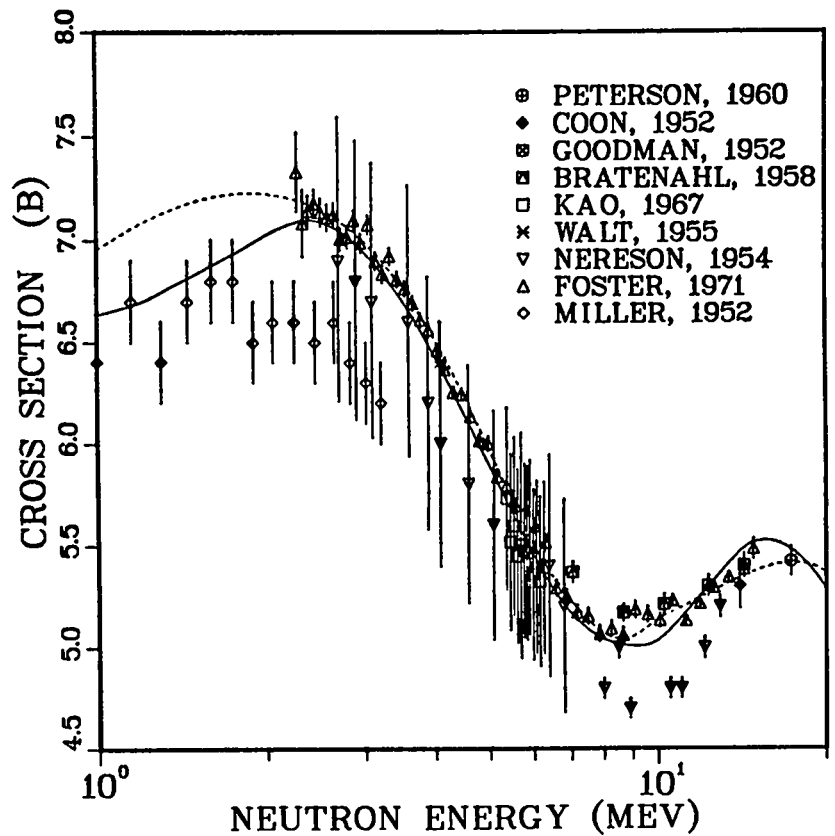


Fig. 9. Evaluated total cross sections for natural tungsten. The dashed curve is ENDF/B-V.

### W-NAT ELASTIC CROSS SECTION

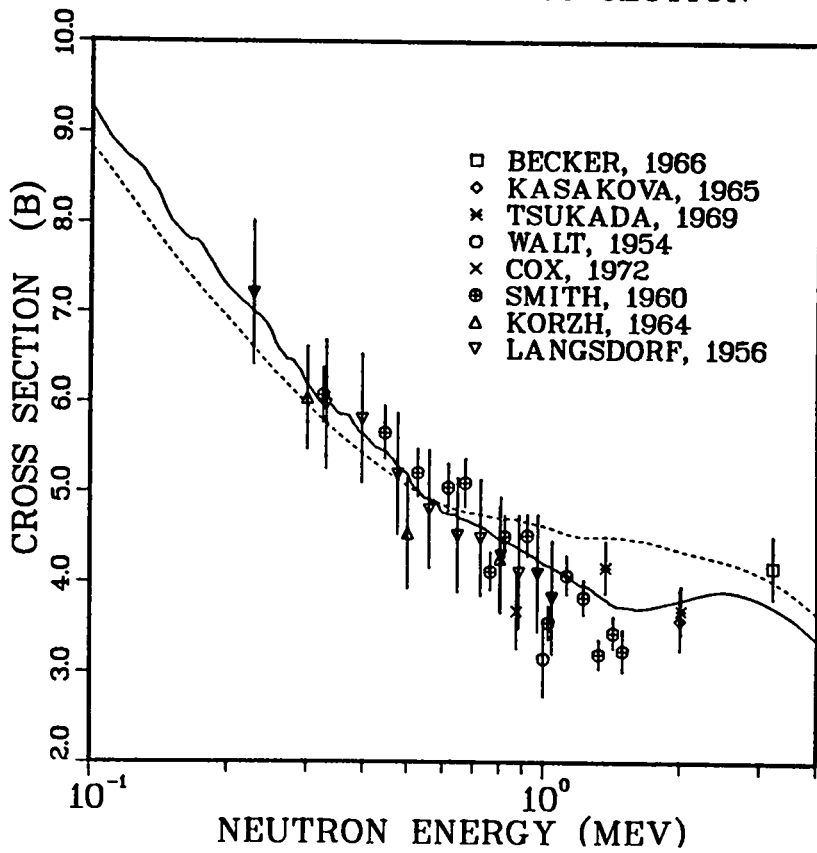


Fig. 10. Evaluated elastic cross sections for natural tungsten. The dashed curve is ENDF/B-V.

### W-NAT ELASTIC CROSS SECTION

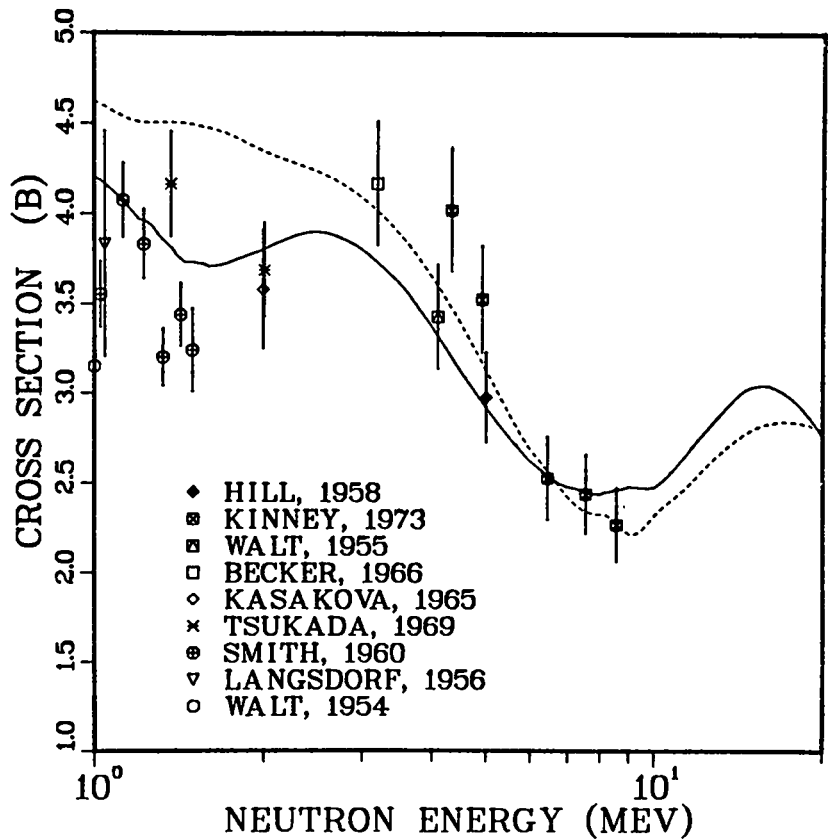
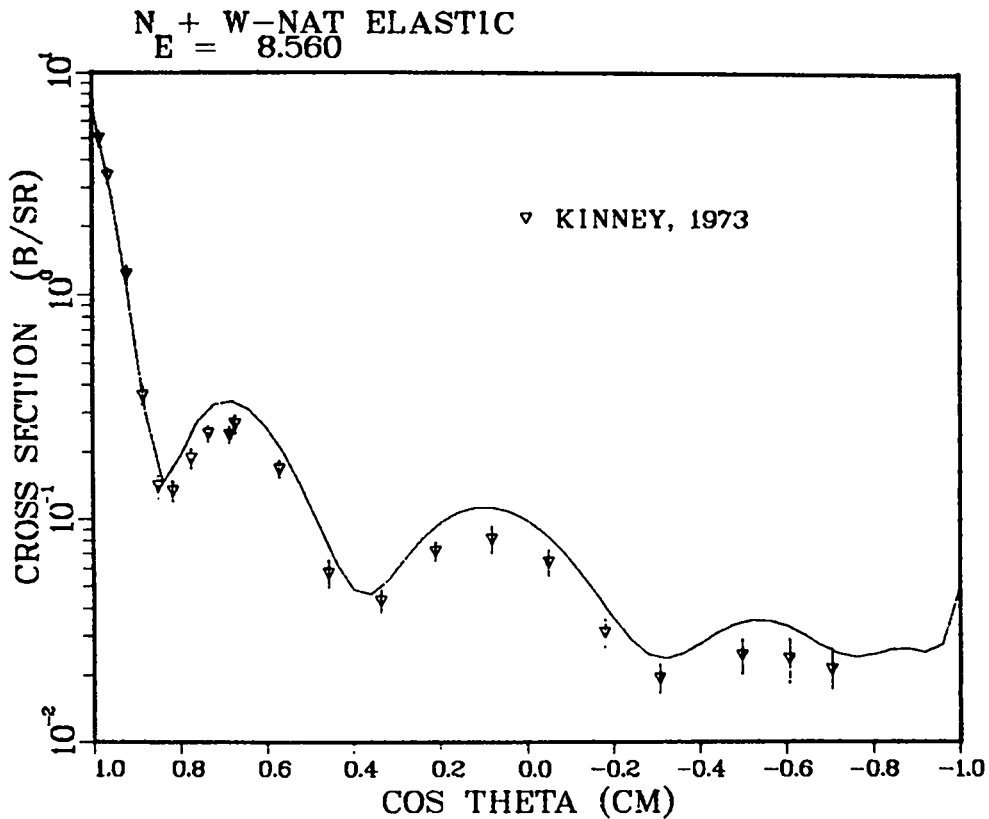
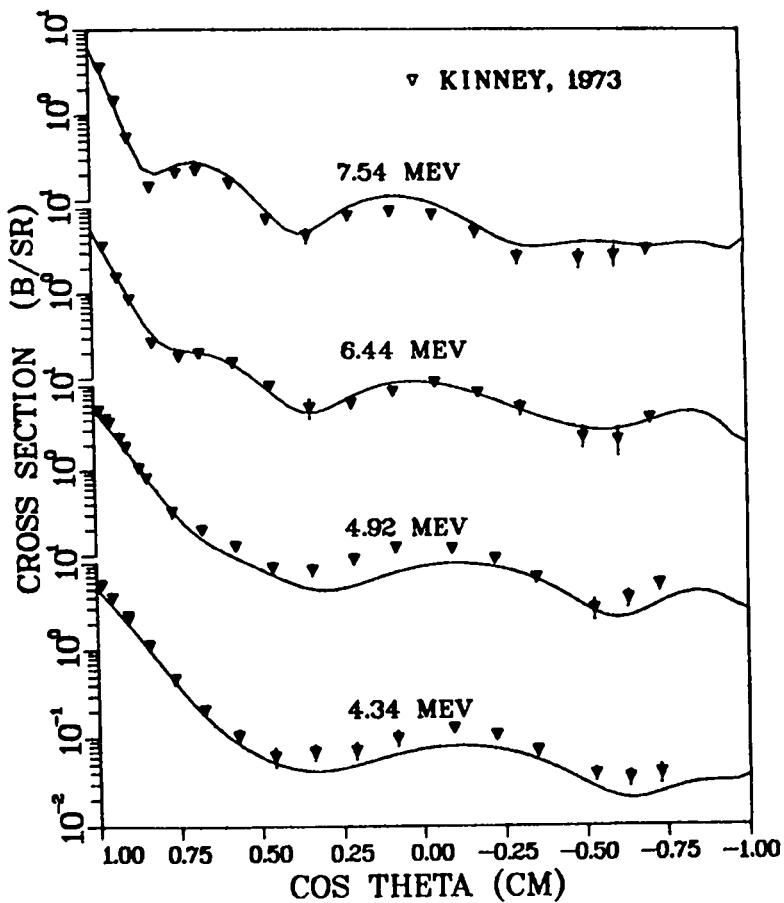


Fig. 11. Comparison of the evaluated angular distributions for elastic scattering (and inelastic scattering producing excitations < 0.1 MeV), and the Kinney measurements.



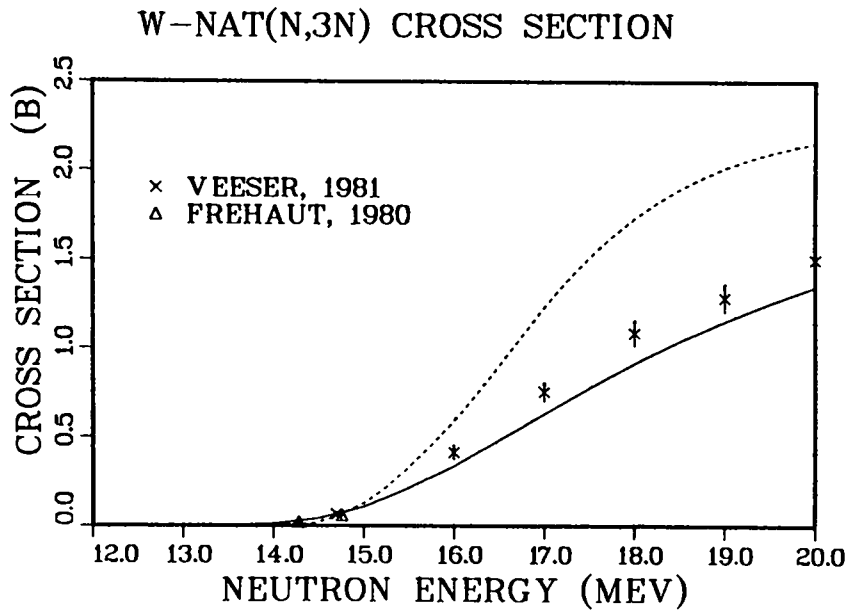
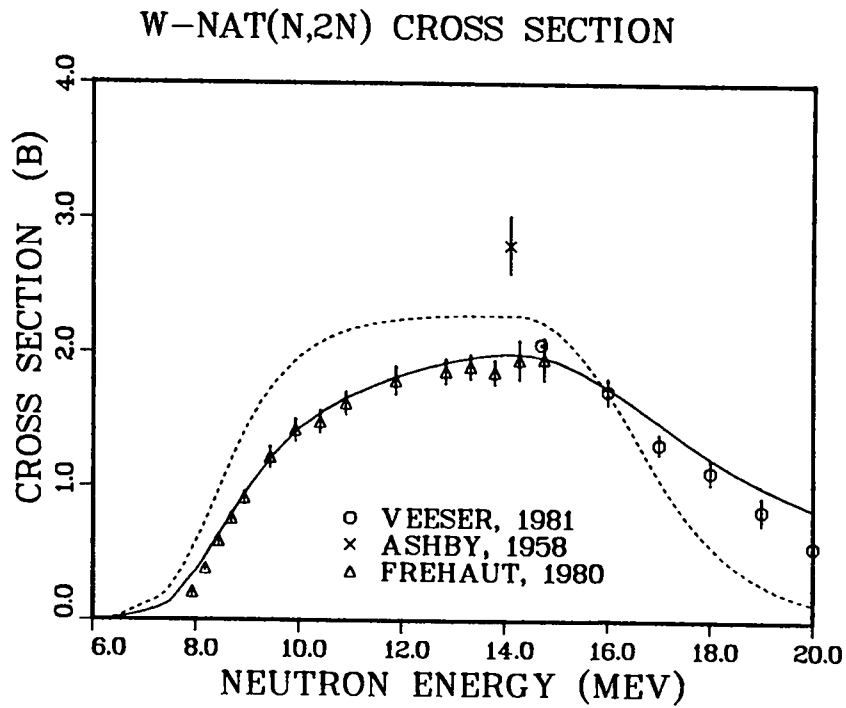


Fig. 12. Evaluated (n,2n) and (n,3n) cross sections are compared to recent experimental data. Again, the solid curve is the present effort; the dashed curve is ENDF/B-V.

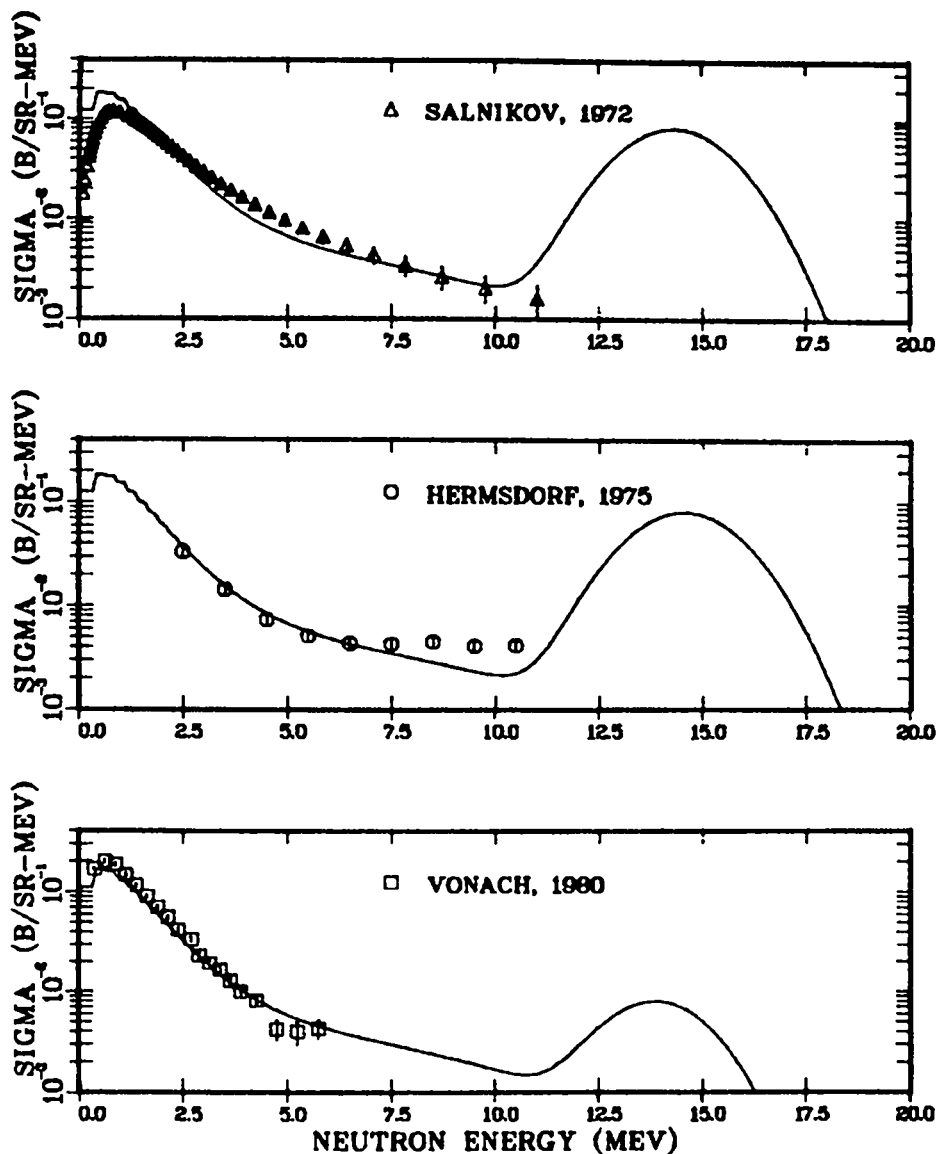
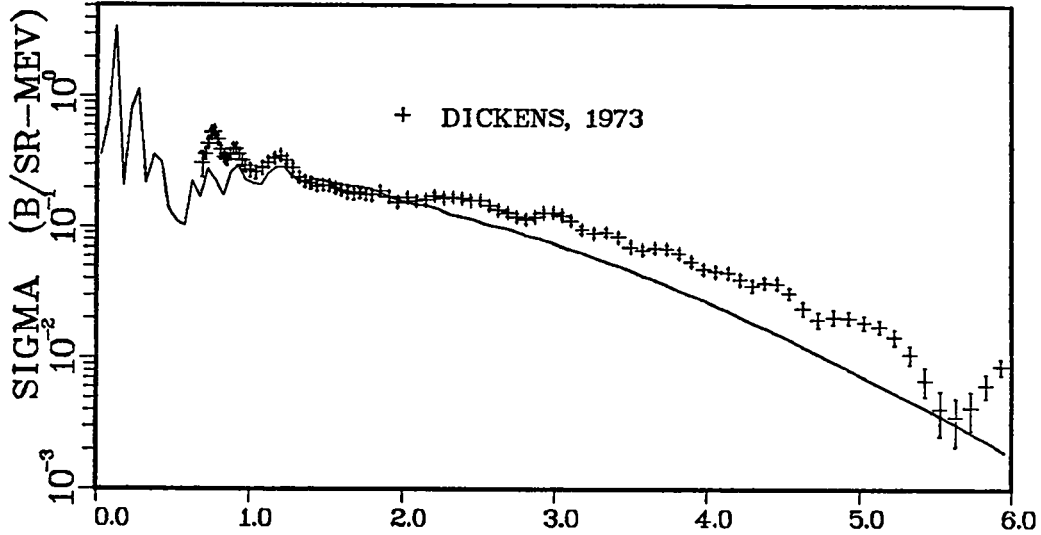


Fig. 13. The evaluated neutron emission spectrum produced by 14-MeV neutrons is compared to experimental results.

Comparisons to the gamma-ray production data of Dickens<sup>24</sup> are shown in Figs. 14-16 for selected incident neutron energy groups. The evaluated gamma-ray production cross sections were obtained from nuclear model calculations to ensure overall energy conservation in the evaluated data files. There are some disagreements to the measurements particularly for gamma rays resulting from continuum inelastic scattering. To some extent this disagreement represents an inconsistency with available neutron cross-section data and is discussed in detail in Ref. 10. We achieve better agreement with the more recent gamma-ray production measurements of Savin,<sup>25</sup> as shown in Figs. 17 and 18, as well as with data measured by Drake.<sup>26</sup>

N + W-NAT PHOTON EMISSION SPECTRA  
E = 7.250



N + W-NAT PHOTON EMISSION SPECTRA  
E = 5.750

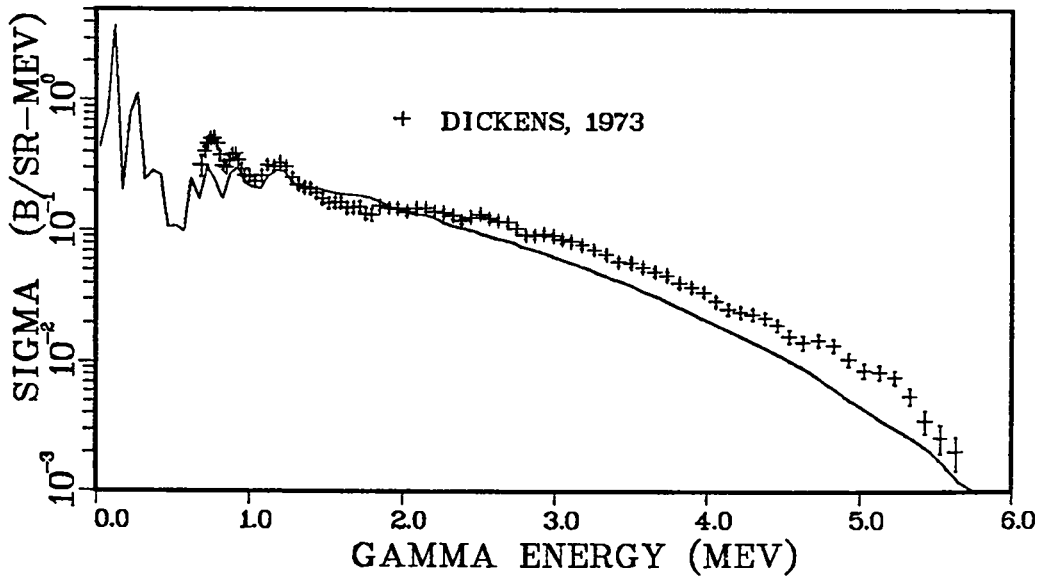
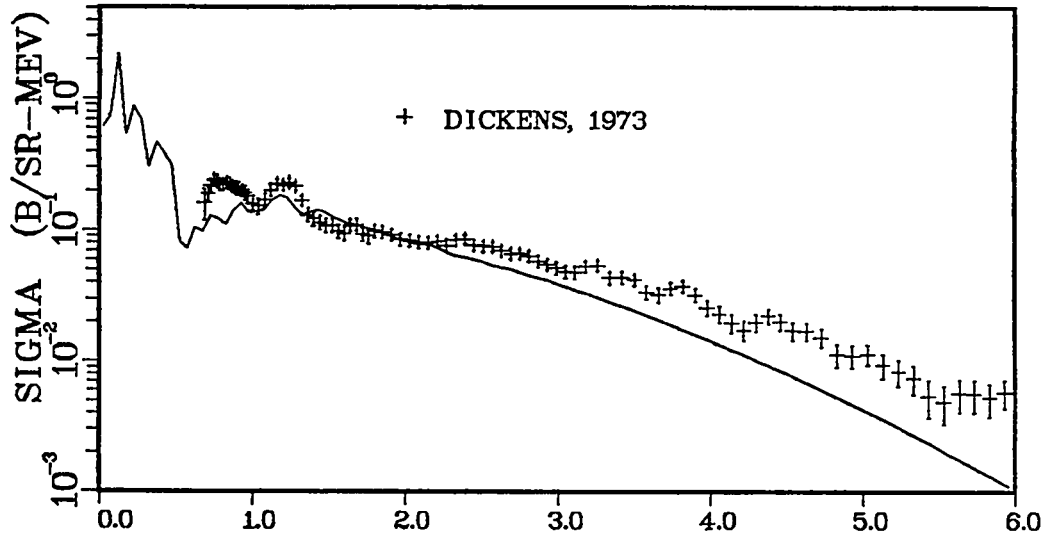


Fig. 14. The evaluated gamma-ray production spectrum obtained in the present effort is compared to Dickens' experimental results.

N + W-NAT PHOTON EMISSION SPECTRA  
E = 9.500



N + W-NAT PHOTON EMISSION SPECTRA  
E = 8.500

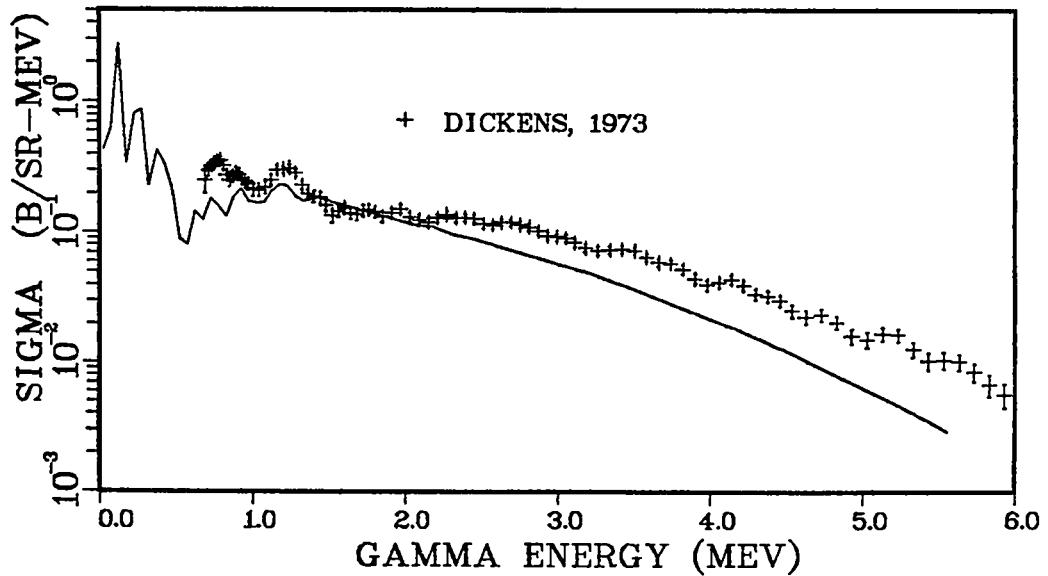
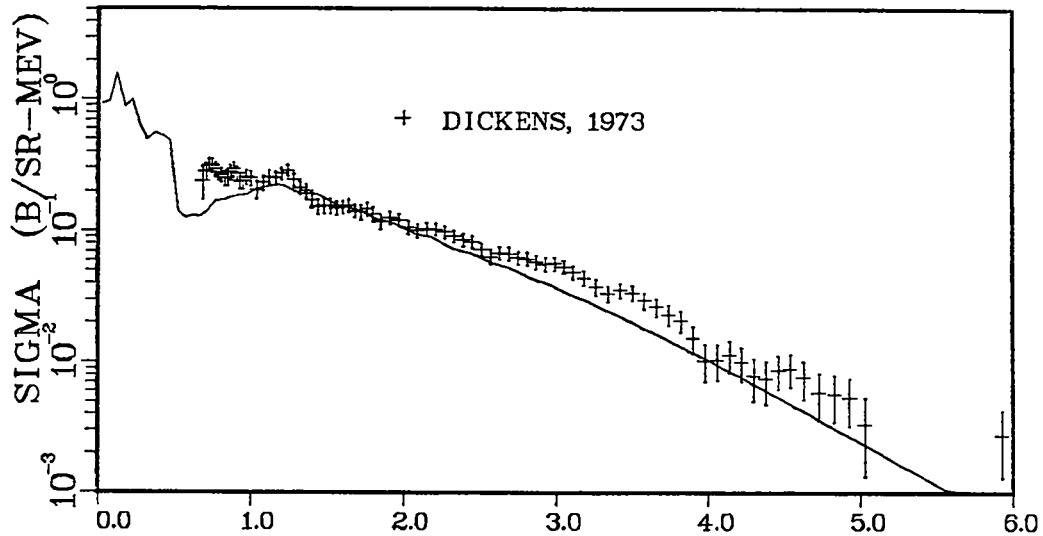


Fig. 15. The evaluated gamma-ray production spectrum obtained in the present effort is compared to Dickens' experimental results.

N + W-NAT PHOTON EMISSION SPECTRA  
E = 13.000



N + W-NAT PHOTON EMISSION SPECTRA  
E = 11.000

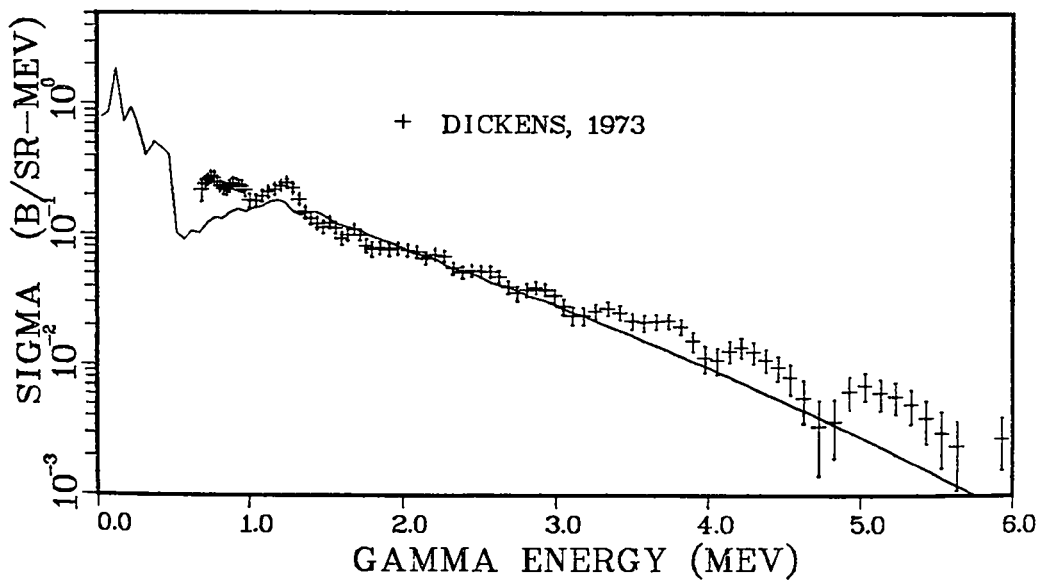
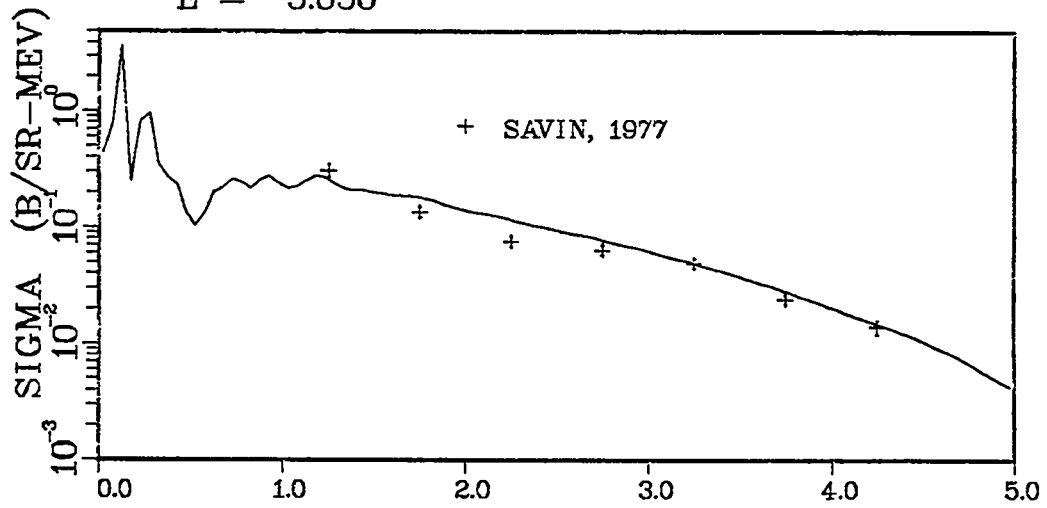


Fig. 16. The evaluated gamma-ray production spectrum obtained in the present effort is compared to Dickens' experimental results.

N + W-NAT PHOTON EMISSION SPECTRA  
E = 5.650



N + W-NAT PHOTON EMISSION SPECTRA  
E = 4.420

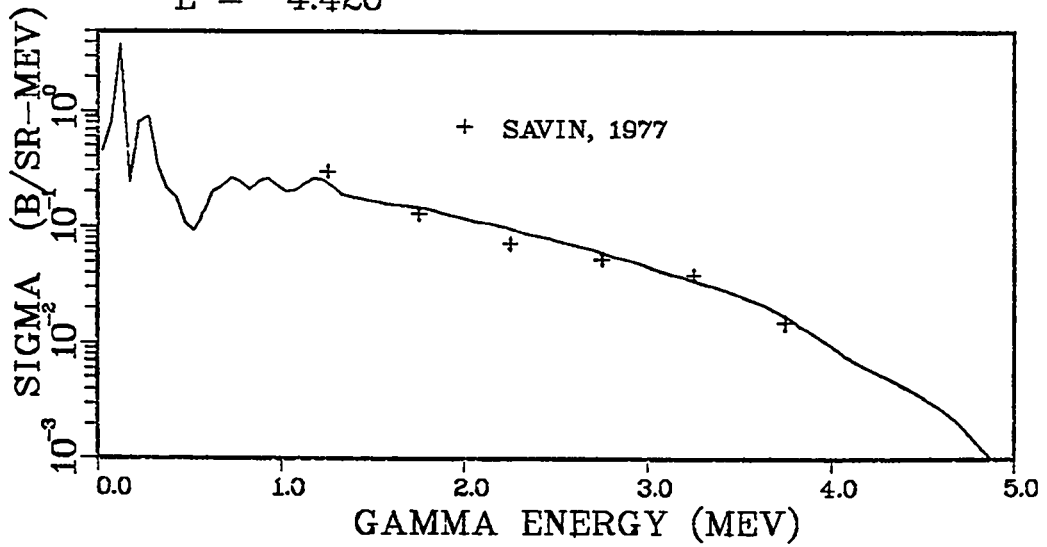
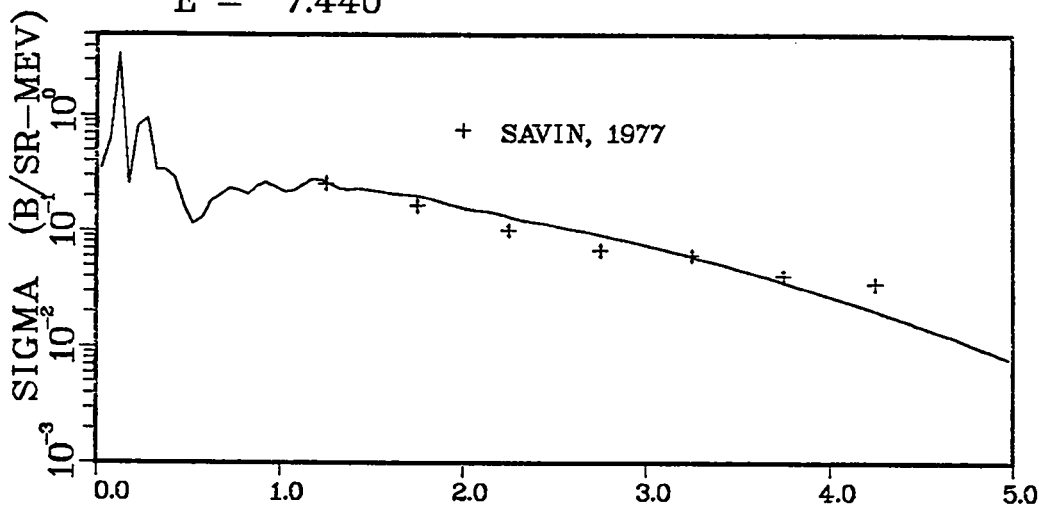


Fig. 17(a). A comparison of the present evaluation to recent gamma production spectra measured by Savin.

N + W-NAT PHOTON EMISSION SPECTRA  
E = 7.440



N + W-NAT PHOTON EMISSION SPECTRA  
E = 6.500

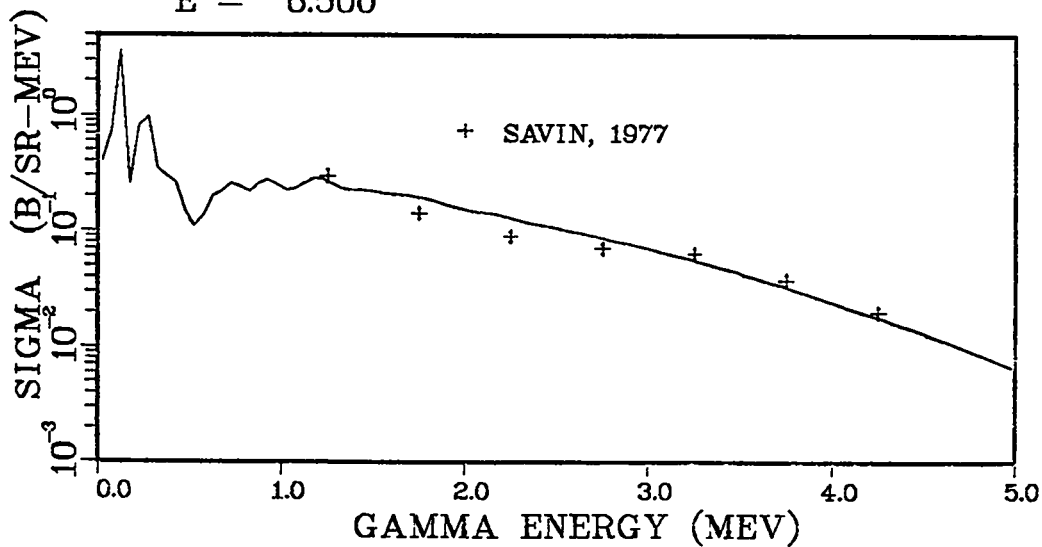


Fig. 17(b). A comparison of the present evaluation to recent gamma production spectra measured by Savin.

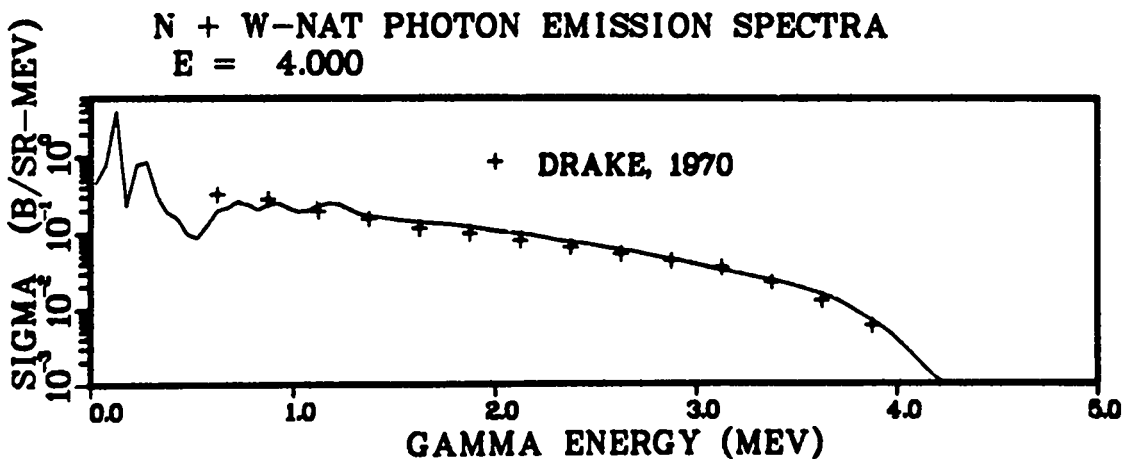
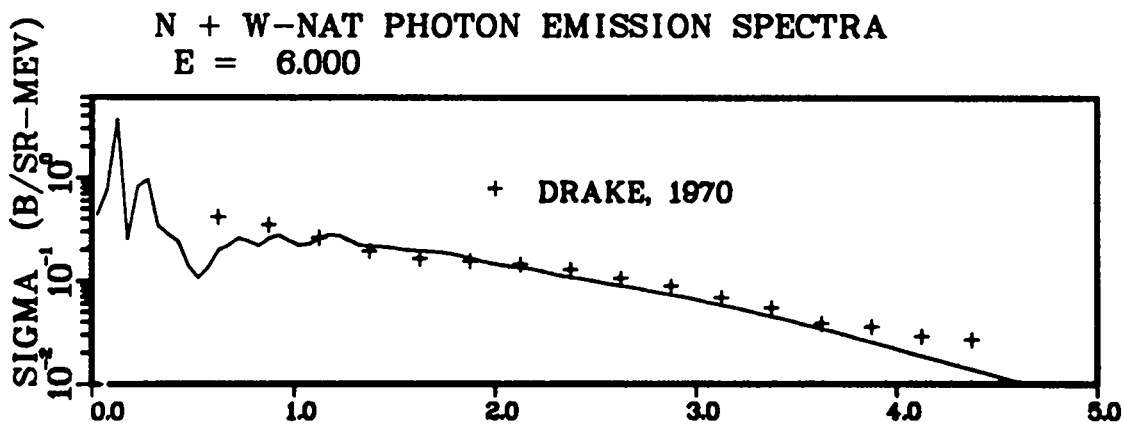
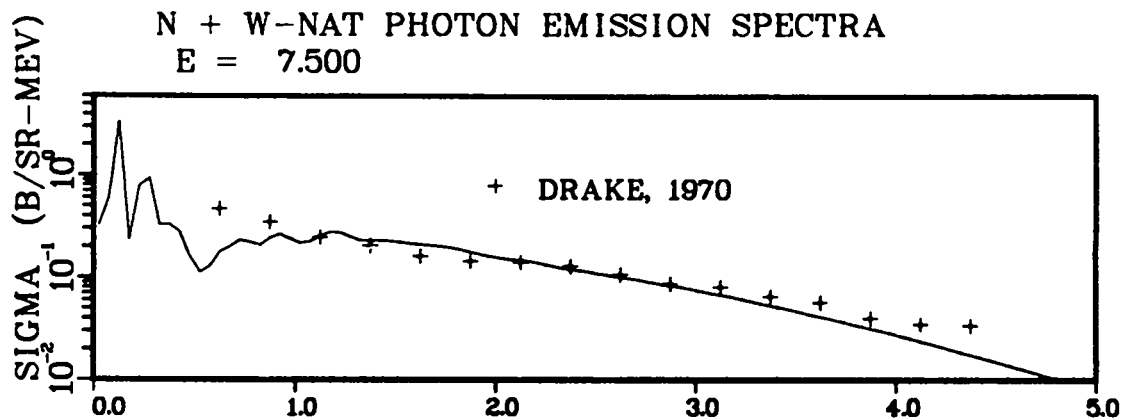


Fig. 18. The present evaluation is compared to the gamma-ray production spectra measured by Drake et al.<sup>27</sup>

H. Application and Further Development of the Improved COMNUC Fission Model  
(E. D. Arthur)

In our previous progress report,<sup>27</sup> we described implementation of an improved fission model in our Hauser-Feshbach statistical model code, COMNUC.<sup>28</sup> We have used this model to calculate neutron-induced fission cross sections on  $^{235,238}\text{U}$  and  $^{239,242}\text{Pu}$  between 0.001 and 5 MeV. A more detailed description of these calculations appears in an invited presentation<sup>29</sup> at the Specialists' Meeting on Fast Neutron Scattering from Actinide Nuclei, Paris, 1981.

As previously described, penetration through the fission barrier is calculated within the code through the use of a three-coupled or two-uncoupled oscillator representation. Furthermore, a spectrum of fission transition states or a continuum of such states must be specified at each barrier to determine the total fission transmission coefficient. To evaluate the continuum of transition states, we use a phenomenological-level density model<sup>30</sup> to which we apply directly an enhancement factor that accounts for symmetry conditions (actually, departures from nuclear symmetry due to deformation effects) existing at each barrier. The enhancements needed at each barrier to reproduce (n,f) data for the nuclei listed above appear in Table II. Also shown in parentheses are results from analyses<sup>31,32</sup> employing transition state densities obtained from microscopic calculations. The agreement is good especially when uncertainties from other barrier parameters are considered. Figure 19 compares our calculated  $^{235}\text{U}(n,f)$  cross section to data available between 0.1 and 5 MeV.

In such calculations corrections must be applied to account for correlations and fluctuations occurring for partial widths used in the Hauser-Feshbach expression for average cross sections. These include width-fluctuation corrections and, in the case of the fission channels, corrections that account for Class II states occurring in the second well. (See Ref. 29 for more details). The effects of such corrections are shown in Fig. 20 for calculated  $^{239}\text{Pu}(n,f)$  cross sections between 0.001 and 5 MeV. For actinide nuclei where fission may not dominate the reaction cross section, these corrections can be equally important. The effects of width fluctuation corrections on the calculated compound elastic and the inelastic scattering cross section to the first excited states in  $^{238}\text{U}$  are illustrated in Fig. 21.

A final segment of our present effort to upgrade the COMNUC fission channel involves addition of a third barrier parallel to the present outer barrier. Such complexity in the fission barrier description has been shown necessary in

order to fit certain fission probabilities obtained from direct-reaction measurements.<sup>33</sup> Additionally, we have modified our method for description of fission transition states so that bandhead information can be supplied at each barrier. This permits the automated construction of the spectrum of such states. These modifications provide more overlap with models used to analyze fission probability measurements so that the extracted barrier parameters can be used with increased confidence in the production of (n,f) cross sections for short-lived target nuclei.

TABLE II

BARRIER ENHANCEMENTS USED FOR (n,f) CALCULATIONS

Compound Nucleus	Barrier A	Barrier B
$^{236}\text{U}$	2. (1.)	2. (2.)
$^{239}\text{U}$	3. (5.)	5. (10.)
$^{240}\text{Pu}$	16. (20.)	2. (2.)
$^{243}\text{Pu}$	18. (20.)	2. (2.)

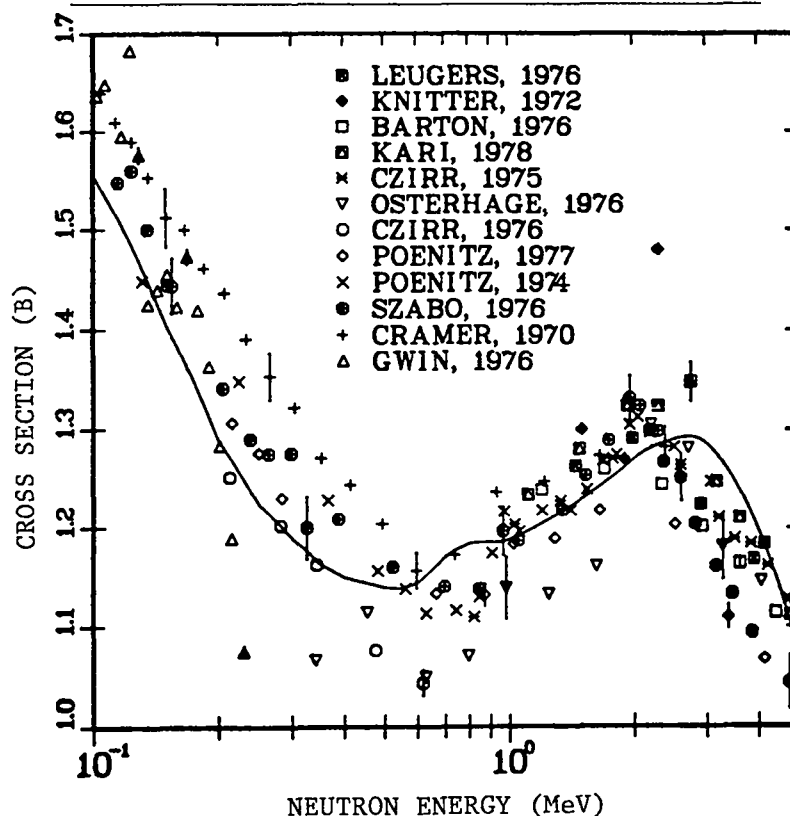


Fig. 19. The calculated  $^{235}\text{U}(n,f)$  cross section is compared to data between 0.1 and 5 MeV.

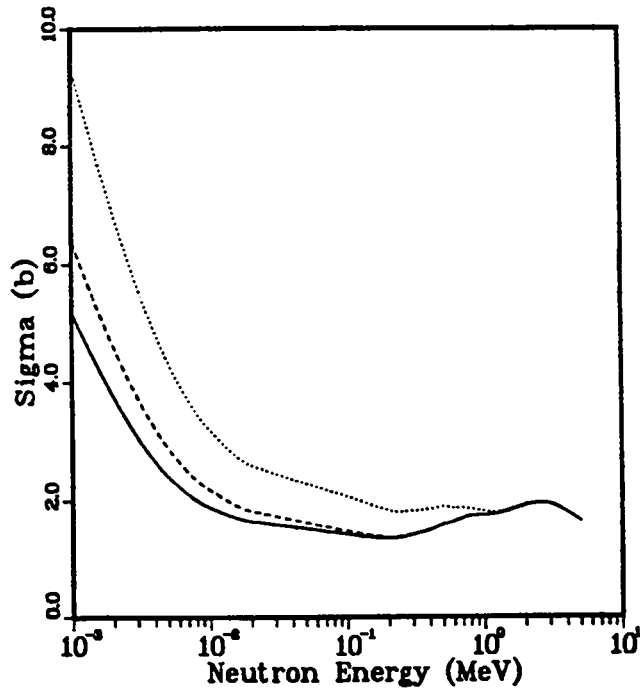


Fig. 20. The effects of fluctuation corrections on calculated  $^{239}\text{Pu}(n,f)$  cross sections are shown. The solid curve includes both width-fluctuation and Class II-fluctuation corrections. The dotted curve ignores both these effects. The dashed curve includes width fluctuations but excludes Class II fluctuations.

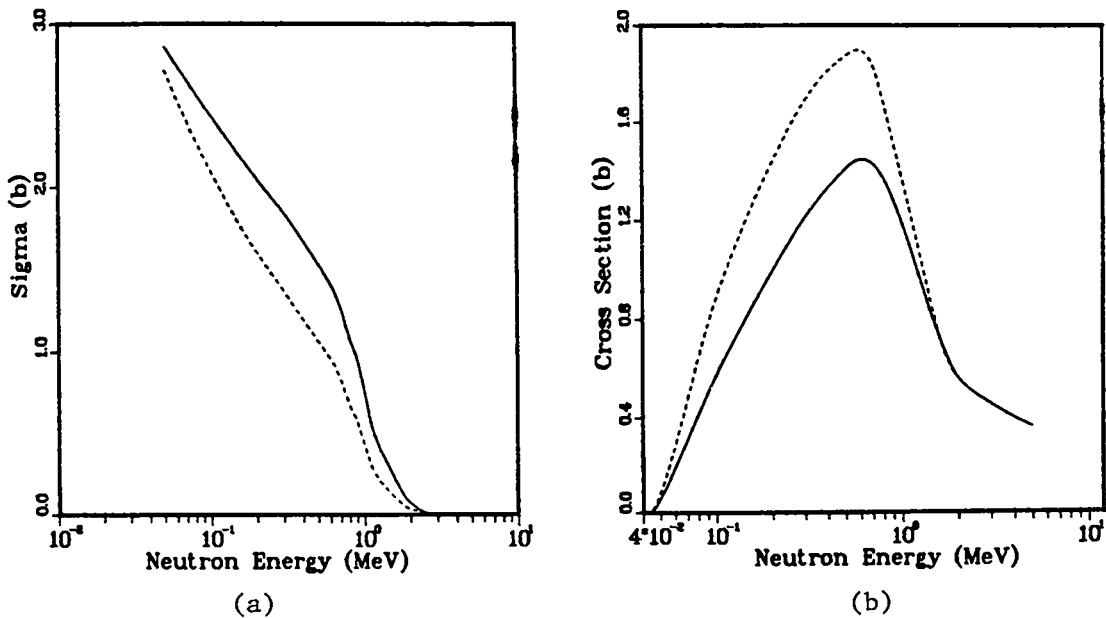


Fig. 21. The effects of width-fluctuation corrections on the calculated (a) compound elastic and (b) inelastic scattering cross section to the 0.045-MeV state in  $^{238}\text{U}$ .

## I. Inelastic Cross Section Calculations on $^{239}\text{Pu}$ (E. D. Arthur)

In order to improve evaluated neutron inelastic scattering cross sections on  $^{239}\text{Pu}$ , we performed coupled-channel direct reaction and Hauser-Feshbach statistical model calculations for neutron energies between 0.01 and 5 MeV. The deformed optical model parameters were described previously,<sup>34</sup> while the statistical model calculations were made with the modified COMNUC code. Cross sections obtained from coupled-channel and compound-nucleus calculations were combined incoherently to produce the desired results. Relevant experimental data for  $^{239}\text{Pu}$  are meager, but our earlier comparisons to recent measurements<sup>35</sup> of 0.7-MeV neutron elastic and inelastic scattering to low-lying levels show good agreement.

Figures 22 and 23 compare our calculated inelastic cross sections for scattering from two low-lying levels in  $^{239}\text{Pu}$  to evaluated data appearing in ENDF/B-V. The large difference between the results for the 0.057-MeV state arises principally because direct-reaction contributions were included in our calculations but not in the ENDF/B-V work. The shape of our calculated excitation function for the 0.164-MeV state occurs because of its relatively high spin (9/2) and because of direct-reaction components. The ENDF/B-V evaluation, on the other hand, probably employs a shape similar to those assumed for scattering from states with lower spin.

Measurements<sup>36</sup> have recently been made at Argonne National Laboratory whereby the total inelastic cross section to levels lying higher than some excitation energy in the target nucleus can be inferred. The threshold for such inelastic excitations varies between 0.08 and 0.3 MeV and occurs because of experimental resolution effects. For our calculations of inelastic scattering on  $^{239}\text{Pu}$ , comparison to such data provides a test of scattering to higher-lying levels that are not members of the ground state rotational band and for which only compound-nucleus contributions were assumed. The solid curve in Fig. 24 compares our calculated values to such data, while the dashed curve represents ENDF/B-V. Our results agree reasonably with the Argonne data but are significantly lower than ENDF/B-V.

Our initial calculations have included direct-reaction contributions only for members of the ground-state rotational band. However, charged-particle experiments<sup>37</sup> show excitation of levels occupying higher-lying bands through direct reaction processes. This is especially true for those levels occurring in the  $K^\pi = 1/2^-$  octupole vibrational band having excitation energies of 0.5-0.6 MeV. As an initial step in determination of direct-reaction components

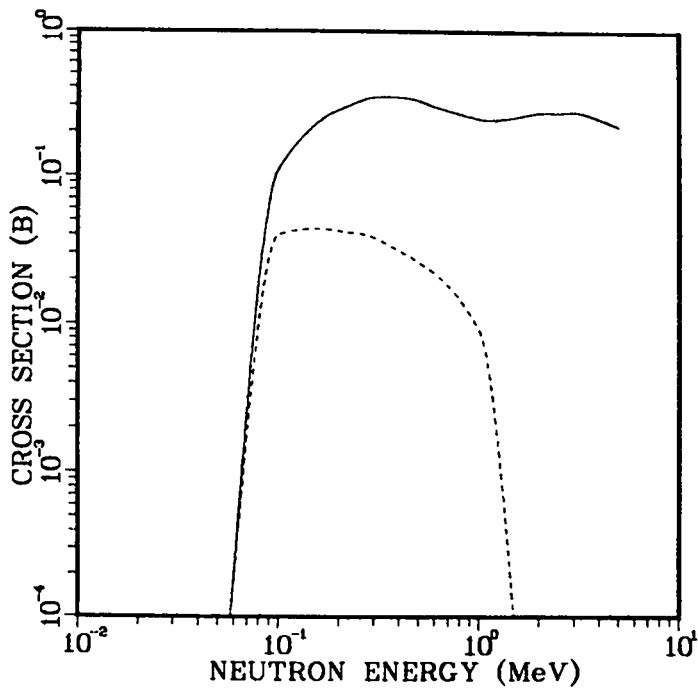


Fig. 22. A comparison of our calculated cross section (solid curve) and that from ENDF/B-V (dashed curve) for excitation of the 0.057-MeV  $5/2^+$  state in  $^{239}\text{Pu}$  through neutron inelastic scattering.

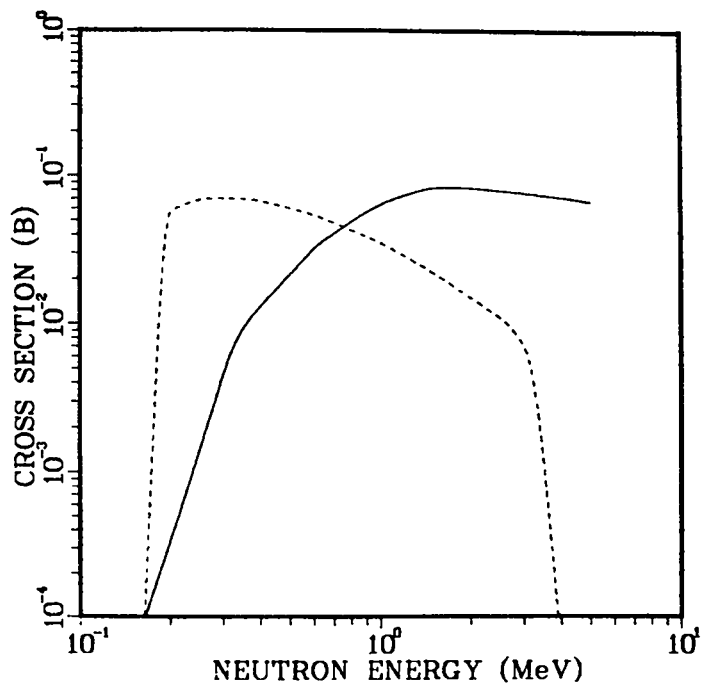


Fig. 23. A comparison of our calculated cross section (solid curve) and that from ENDF/B-V (dashed curve) for excitation of the 0.164-MeV  $9/2^+$  state in  $^{239}\text{Pu}$  through neutron inelastic scattering.

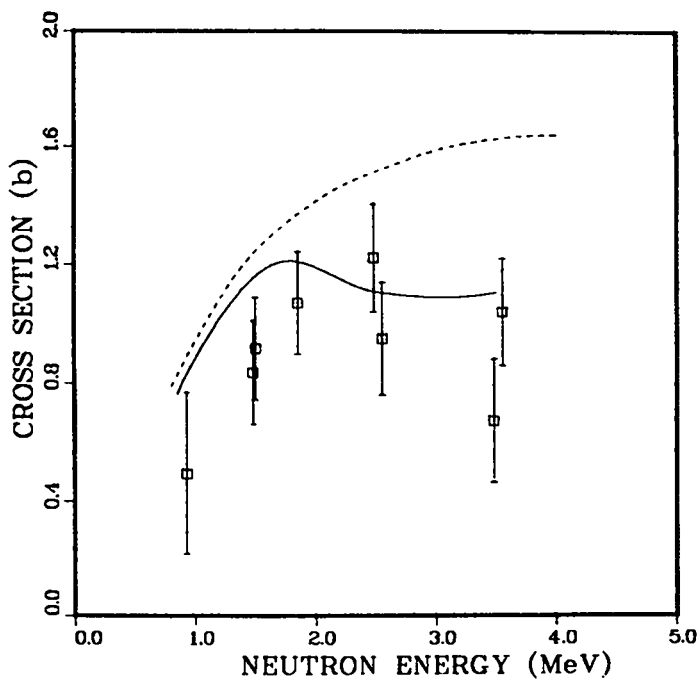


Fig. 24. Comparison of the present calculated "total inelastic" (solid curve) to new measurements by A. Smith, ANL, and to ENDF/B-V (dashed curve).

in neutron inelastic scattering from such states, we performed Distorted Wave Born Approximation (DWBA) calculations for scattering from the 0.555-MeV  $7/2^-$  state assuming an  $\ell = 3$  angular momentum transfer. The Madland-Young optical model parameters<sup>38</sup> were used, while the normalization for the calculated results was obtained from  $\beta_3$  values based on measured B(E3) results for octupole states in nearby nuclei.<sup>39</sup> Our direct-reaction cross sections obtained in this manner were only approximately of 5-10 mb for  $E_n = 3$  MeV. These results are in apparent disagreement to (n,n') cross sections for scattering from octupole states in  $^{238}\text{U}$  and  $^{232}\text{Th}$ , as deduced from (n, n' $\gamma$ ) measurements<sup>40,41</sup> on these nuclei.

To further test our calculations, we analyzed charged-particle data for (d,d') and (p,p') measurements of scattering from the 0.731-MeV  $3^-$  octupole state in  $^{238}\text{U}$ . We obtained an overall normalization which was then applied to our  $\ell = 3$  DWBA calculations. Our  $\beta_3$  values obtained in this manner again agreed with B(E3) results and produced neutron inelastic scattering cross sections significantly smaller than those deduced using the (n,n' $\gamma$ ) measurements. Figure 25 compares our calculated results for scattering from the 0.731-MeV state in  $^{238}\text{U}$  to the data of Olsen<sup>41</sup> obtained via the (n,n' $\gamma$ ) technique.

The disagreement between our calculations and these experimental results indicate a possible inconsistency between the neutron data and charged-particle B(E3) values. An experiment is now planned to help resolve this discrepancy through measurement of (p,p') angular distributions from these levels in  $^{238}\text{U}$  and  $^{239}\text{Pu}$ .

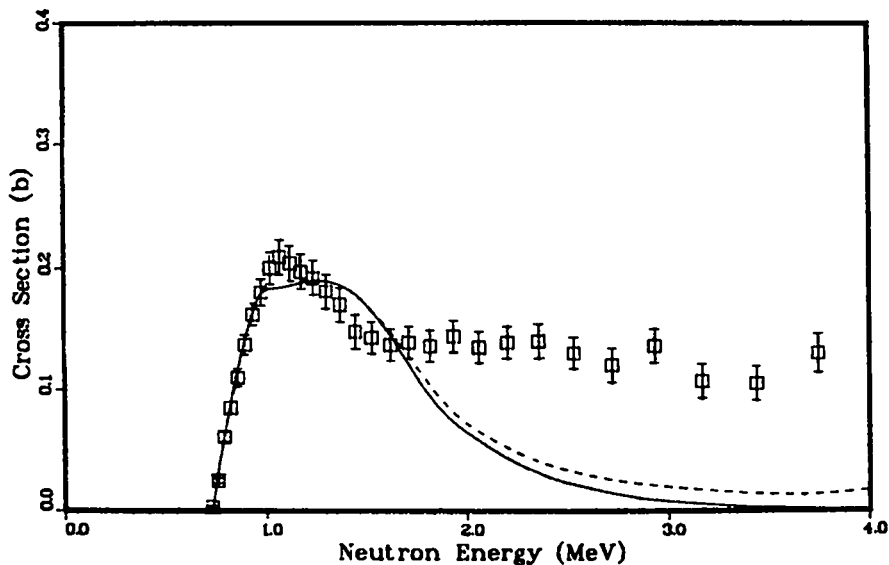


Fig. 25. Comparison of the calculated (n,n') cross section for excitation of the 0.731-MeV  $3^-$  octupole state in  $^{238}\text{U}$ . Both compound nucleus and direct-reaction (DWBA) components are included in the dashed curve; the solid curve is the compound nucleus contribution alone. The data are those of Olsen<sup>41</sup> deduced from (n,n' $\gamma$ ) measurements.

J. New Calculation of Prompt Fission Neutron Spectrum  $N(E)$  and Average Prompt Neutron Multiplicity  $\bar{\nu}_p$  [D. G. Madland and J. R. Nix (T-9)]

An extensive manuscript summarizing this work has been accepted for publication in Nuclear Science and Engineering.<sup>42</sup> The manuscript marks the completion of our presentation of the new theory of  $N(E)$  and  $\bar{\nu}_p$  that we have developed.

K. New Fission Neutron Spectrum Representation for ENDF (D. G. Madland)

A new representation of the prompt fission neutron spectrum has been proposed for use in the Evaluated Nuclear Data File (ENDF). The proposal has been made because a new theory exists<sup>42</sup> by which the spectrum can be accurately predicted as a function of the fissioning nucleus and its excitation energy. Thus, prompt fission neutron spectra can be calculated for cases where no measurements exist or where measurements are not possible.

The simplest form of the new theory is used, namely, the constant compound-nucleus cross-section approximation.<sup>42</sup> This is done because the resulting expressions for the spectrum and its integral over arbitrary energy range are of closed form, with only slight compromises in accuracy. The proposal document<sup>43</sup> presents the mathematical formalism necessary for application of the theory within the ENDF structure and treats neutron-induced fission and spontaneous fission. In the case of neutron-induced fission, expressions are given for the first-chance, second-chance, third-chance, and fourth-chance fission components of the spectrum together with that for the total spectrum. An ENDF format is provided for the new fission spectrum representation, and an example of the use of the format is given.

L. Calculation of the Prompt Neutron Spectrum and Average Prompt Neutron Multiplicity for the Spontaneous Fission of  $^{252}\text{Cf}$  [D. G. Madland and J. R. Nix (T-9)]

On the basis of a new theory<sup>42</sup> of the prompt fission neutron spectrum  $N(E)$  and average prompt neutron multiplicity  $\bar{\nu}_p$ , we are calculating these quantities for the spontaneous fission of  $^{252}\text{Cf}$ . We are studying this particular reaction because it is used as a standard in many measurements and applications of neutron physics.

In order to calculate  $N(E)$  and  $\bar{\nu}_p$  with high accuracy, we require highly accurate values of the average fission energy release  $\langle E_r \rangle$ , the total average fission-fragment kinetic energy  $\langle E_f^{\text{tot}} \rangle$ , the nuclear level-density parameter  $a$ ,

the total average prompt gamma energy  $\langle E_{\gamma}^{\text{tot}} \rangle$ , and the average fission-fragment neutron separation energy  $\langle S_n \rangle$ . Whereas for  $^{252}\text{Cf}$ ,  $\langle E_f^{\text{tot}} \rangle$  and  $\langle E_{\gamma}^{\text{tot}} \rangle$  are measured quantities and  $a$  is inferred from measurements, the average energy release  $\langle E_r \rangle$  and the average fission-fragment neutron separation energy  $\langle S_n \rangle$  must be calculated. In our previous work<sup>42,44</sup> we have calculated  $\langle E_r \rangle$  and  $\langle S_n \rangle$  by use of a seven-point approximation to their integrals over the fission-fragment mass and charge distributions, using measured or systematic masses of Wapstra and Bos<sup>45</sup> when they exist, and otherwise the droplet-model mass formula of Myers.<sup>46</sup> In this work, because of the increased accuracy requirements, we are performing the required integrations without approximation and are using the mass formula of Möller and Nix<sup>47</sup> for determining unmeasured masses. The subroutine QVAL has been constructed for the latter purpose. A call to QVAL results in a search for the desired mass first from the Wapstra and Bos<sup>45</sup> mass table and, if not found, second from the Möller and Nix<sup>47</sup> mass table. With these improvements we calculate  $N(E)$ ,  $\bar{\nu}_p$ , and the decomposition of  $\bar{\nu}_p$  into  $\bar{\nu}_p(A)$ , where  $A$  is the mass number of either the light or the heavy fragment.

Two results have been obtained thus far, but these are preliminary because (a) the fission-fragment mass and charge distributions used in the integrations have yet to be finalized, and (b) the experimental values used for  $E_f^{\text{tot}}(A)$  and  $E_{\gamma}^{\text{tot}}(A)$ , that is, the decomposition of  $\langle E_f^{\text{tot}} \rangle$  and  $\langle E_{\gamma}^{\text{tot}} \rangle$ , have to be understood more completely. Keeping these points in mind, our preliminary results are

1.  $\bar{\nu}_p [^{252}\text{Cf}(\text{sf})] = 3.770$ , to be compared with the current accepted value of  $3.757 \pm 0.009$ , and
2. agreement to within approximately 5% with the  $\bar{\nu}_p(A_H)$  experimental data of Boldeman and Walsh,<sup>48</sup> where  $126 \leq A_H \leq 164$ .

M. Calculation of Excited-State Cross Sections for Actinide Nuclei (D. G. Madland)

Further improvements and studies of the coupled-channel excited-state target code JUPXST have been made in preparation of calculating excited-state transmission coefficients for three- and four-state coupling. These are

1. A direct test of the unitarity of the full coupled-channel  $S$  matrix in the limit of no absorptive potential with the results that the calculated off-diagonal elements of  $S$  are zero to within a few parts in  $10^7$  and that

the corresponding transmission coefficients are zero to a precision approaching a few parts in  $10^{13}$ .

2. A test of reciprocity between  $0^+ \rightarrow 2^+$  and  $2^+ \rightarrow 0^+$  coupling with the result, after certain numerical improvements, that reciprocity is satisfied to within a few parts in  $10^7$ .
3. Additional convergence tests for incident neutron energies that are below the excitation energy of the highest coupled target state. Here we have results that are not yet understood, namely, matching radius dependencies of the calculated sub-threshold cross sections and the behavior of the S matrix in the sub-threshold region. We are presently continuing our studies in the sub-threshold region, which is an important one for certain excited-state target calculations.

## II. NUCLEAR CROSS-SECTION PROCESSING AND TESTING

### A. NJOY Code Development (R. E. MacFarlane, D. W. Muir, and R. M. Boicourt)

A new version of the NJOY nuclear data processing system called NJOY (10/81) has been released to the national code centers and interested individual users. This code is widely used for preparing neutron and photon cross sections from evaluated data in ENDF/B format. The new version corrects a number of errors and adds several new capabilities.

The resonance reconstruction module (RECONR) now supports analytic psi-chi Doppler broadening for the Adler-Adler resonance representations as well as the single-level Breit-Wigner form, control of significant digits has been improved, and an extended resonance reconstruction algorithm<sup>49</sup> has been introduced. In the Doppler broadening module (BROADR), an error that affected low-energy cross sections at high temperatures was repaired, and more control over the energy range for broadening was added to avoid pathological results for cross sections containing sharp steps or resonances represented as triangles (for example, ENDF/B-V lead).

The UNRESR unresolved-resonance calculation was changed to guarantee compatibility between the smooth cross sections in File 3 and the self-shielded numbers in File 2. In the HEATR module, an option to compute radiation-damage energy production<sup>50</sup> was added. In addition, the existing heat production calculation was modified to use momentum balance to compute the recoil for radiative capture.<sup>50</sup> This gives better results for capture heating at low energies, which is difficult to compute well as the difference between two large numbers.

It also gives reasonable results for elements, which cannot be handled by energy balance because the available energy is not given in the ENDF/B files. Unfortunately, total energy is no longer explicitly conserved.

The thermal treatment (THERMR) is now based on the use of discrete angles rather than Legendre coefficients. A representation using eight equally probable angles can be converted to multigroup Legendre data as good as the results of the old  $P_3$  method when the angular variation is modest, and it gives much better results when the scattering is concentrated into a small angular range (which is common in practice). For coherent elastic scatter (for example, graphite), the discrete angles and their weights can be determined directly from the positions and magnitudes of the Bragg edges in the cross section; therefore, the higher moments are no longer calculated. Similar methods are used for incoherent elastic scattering. For the convenience of the user, default effective temperatures for the short-collision-time approximation have been added for use in extending the ENDF/B data to higher energy and momentum transfers.

In the multigroup module (GROUPE), the background cross sections list can now be different from the list in UNRESR. The flux calculator has been improved at the cost of requiring extended memory, and it now includes the capability for representing intermediate-resonance effects due to admixed oxygen and external hydrogen and oxygen using a two-region approximation.<sup>51</sup> More group structures and weight functions have been added, and several improvements have been made to the calculation of fission spectra. The photon interaction module (GAMINR) has a new group structure. The recommended weight function has been changed to  $1/E$  with high- and low-energy roll offs.

The (10/81) version of the ERRORR module for processing the ENDF/B covariance files includes several new capabilities, including the treatment of cross-material covariances, fission  $\bar{\nu}$  uncertainties, and resonance-parameter covariances. The new COVR module is also included in this version. It makes high-quality plots of uncertainties and correlations.<sup>52</sup> Some more recent developments in ERRORR and COVR (to be included in a later version of NJOY) are described elsewhere in this report.

The CCCC output module has been updated to the CCCC-IV specifications.<sup>53</sup> Fission matrices are now available, and fission vectors can be computed for an input flux if desired. The self-shielding factor file now includes sub-blocking and elastic removal shielding factors. The MATXS output modules have been updated to include some new reaction names for ENDF/B-V.

Because the input for NJOY(10/81) and certain aspects of the code operation are different from the earlier versions, a new users' manual has been issued. The new manual is available as Volume I of Los Alamos National Laboratory report LA-9303-M.<sup>4,54</sup> Volume I is intended to replace the previous manual, LA-7584-M. Volume II of the new report, which is also complete, provides detailed descriptions of the NJOY module (containing the executive program and utility subroutines used by other modules), and it discusses the theory and computational methods of four of the modules used for producing pointwise cross sections: RECONR, BROADR, HEATR, and THERMR. Future volumes describing the groupwise and covariance modules are also planned.

A more formal procedure has been adopted for communicating changes to the expanding NJOY user community. A mailing list has been established for a series of "NJOY Notes." Notes 1 and 2 have already been issued. They provide corrections to a number of errors found in testing and a group of changes that improves IBM compatibility. Persons interested in being placed on the mailing list to receive these and future Notes should contact the code authors. As a result of IBM testing carried out by C. Stenberg at the Argonne National Laboratory, an IBM version of NJOY has been released to the code centers.

B. New 80-Group Fast Reactor Cross-Section Library (R. B. Kidman, R. E. MacFarlane, R. M. Boicourt)

A new multigroup cross-section library has been prepared using ENDF/B-V evaluated data and the NJOY processing system. The library is intended to be used for fast reactor analysis and benchmark calculations; but, with due care, it is also useful for many fusion and shielding problems.

The weight function and 80-group structure for the library are shown in Figs. 26-26b. The weight function is based on the smoothed core spectrum for a typical large LMFBR benchmark with a fusion peak added at high energies and a 1/E plus thermal tail added at low energies. This tail is intended to improve the results of calculations in the outer regions of the reactor without requiring an unreasonable shape through the keV region important in the core. The group structure is similar to our previous 70-group set, with more low-energy groups, more fusion groups, and one more boundary in the region of the 27-keV iron resonance.

The library contains neutron scattering, photon production, and photon interaction data, including Legendre coefficients to order 5. Self-shielding is

OVERALL WEIGHT FUNCTION

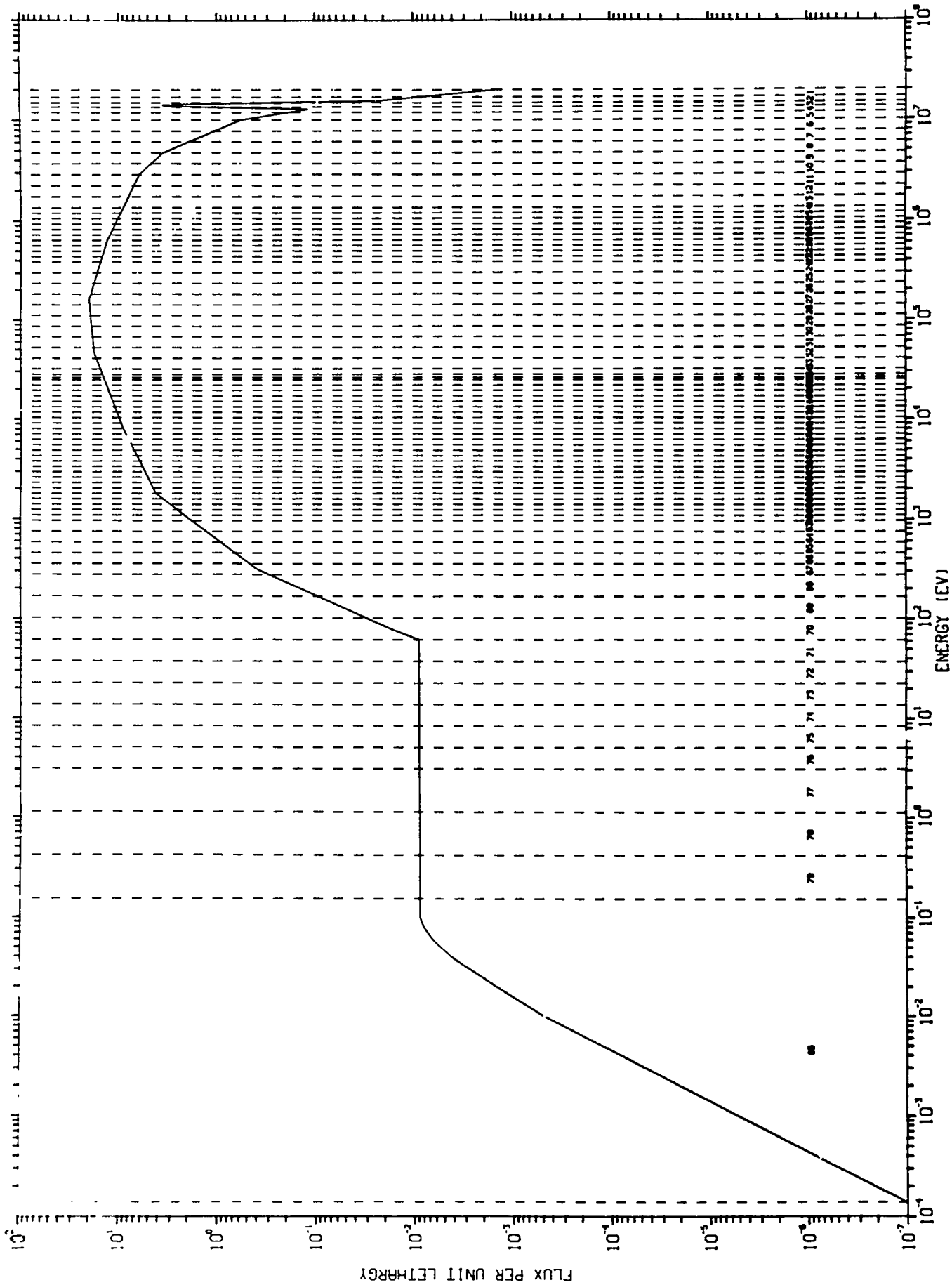


Fig. 26. Weight function and 80-group structure for the new fast reactor cross-section library.

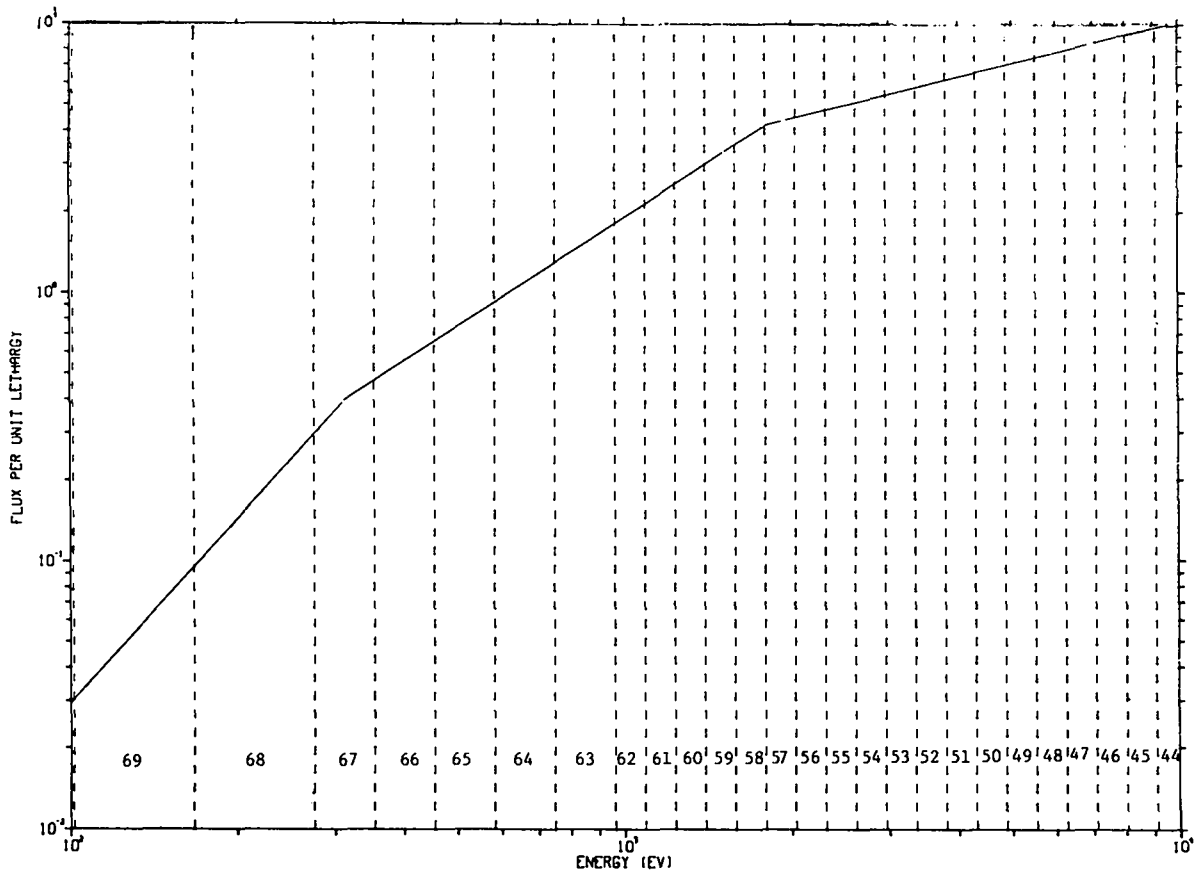
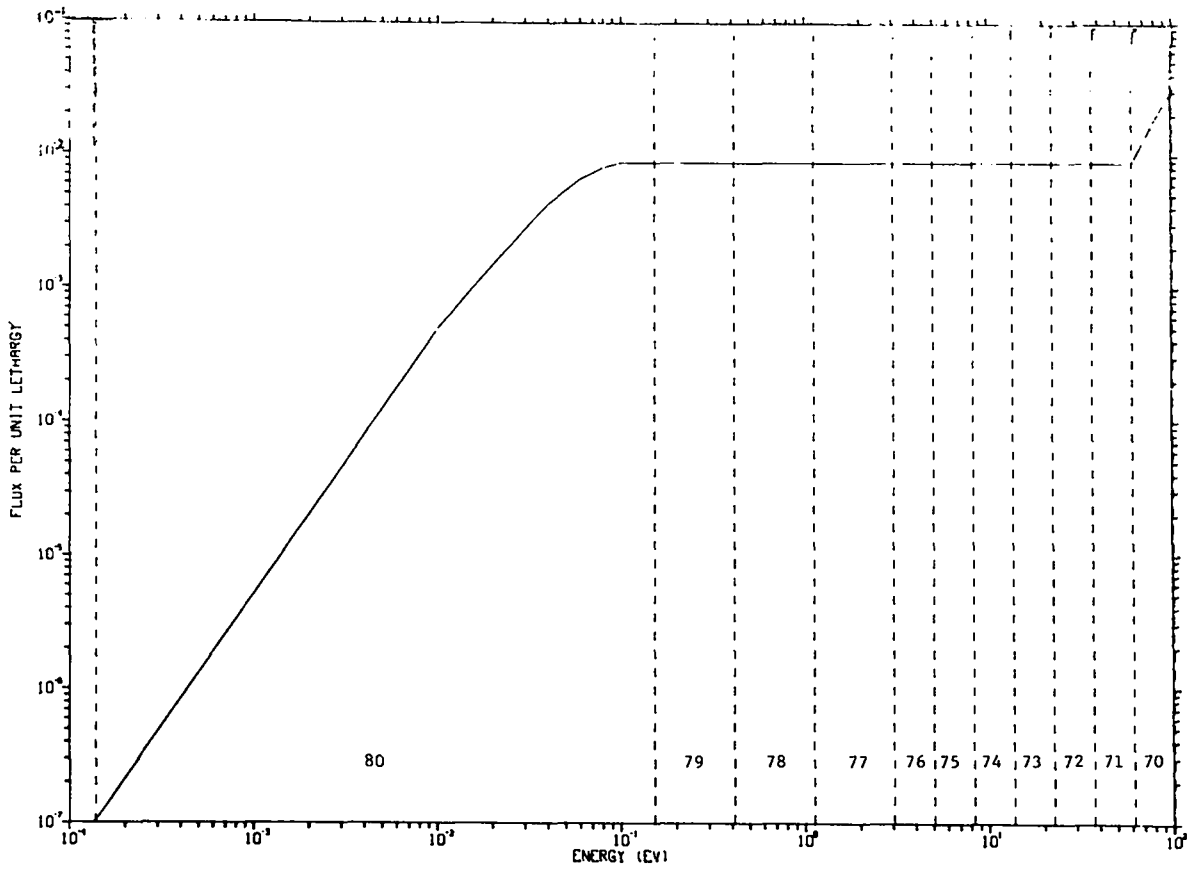


Fig. 26a. Enlargements of the first two sections of the weight function and 80-group structure for the new fast reactor cross-section library (Fig. 26).

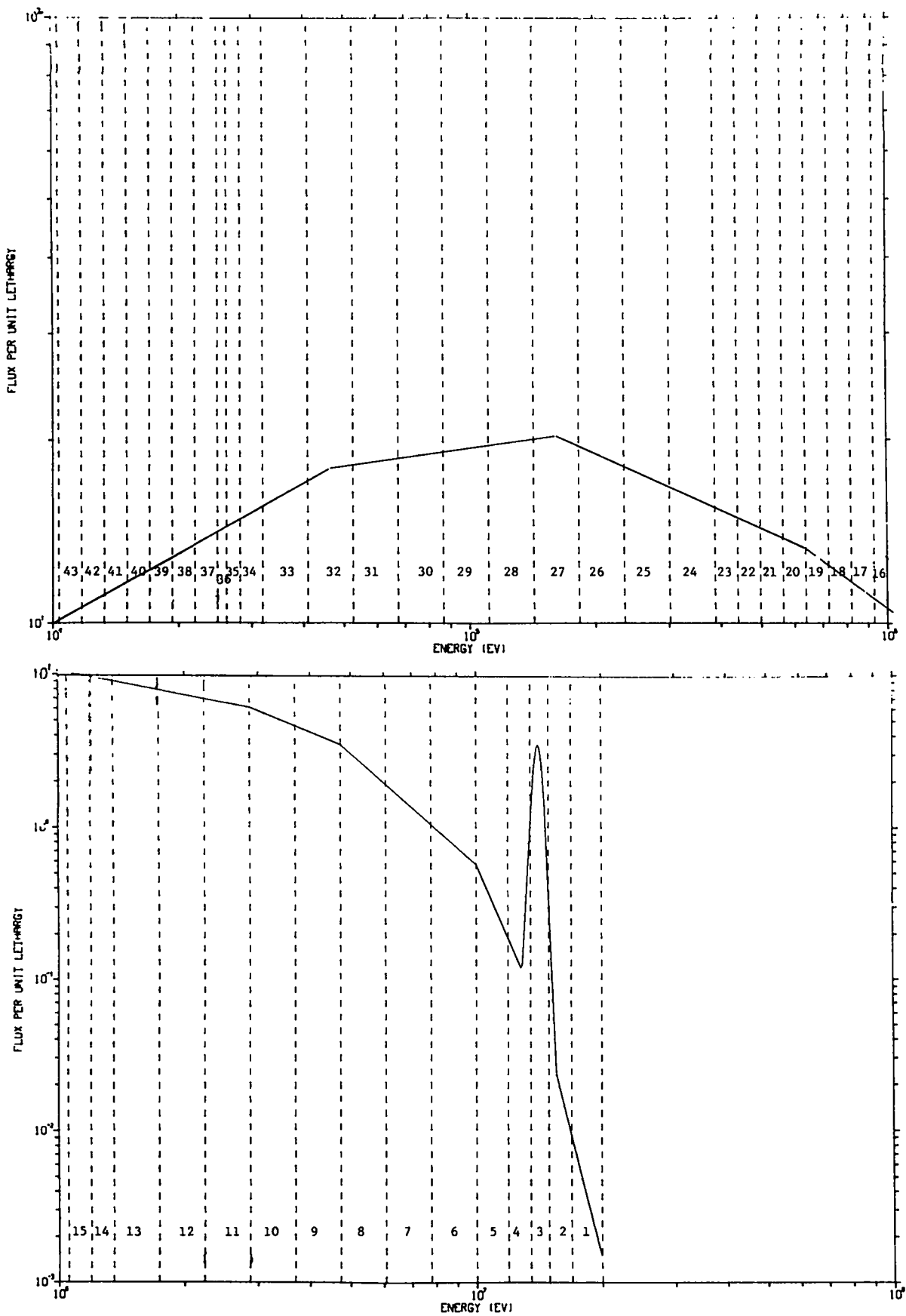


Fig. 26b. Enlargements of the last two sections of the weight function and 80-group structure for the new fast reactor cross-section library (Fig. 26).

given, in some cases for temperatures as high as 8000° K. Heating and radiation damage cross sections are also available. Fission matrices and delayed neutron parameters are included.

The library is available in the CCCC-IV interface format<sup>55</sup> files ISOTXS, BRKOXS, and DLAYXS, and in the new MATXS format. The CCCC files do not include the photon, heating, and radiation damage data. The MATXS file does not include the delayed neutron data.

C. NJOY Covariance Modules, ERRORR and COVR (D. W. Muir, R. M. Boicourt, and R. E. MacFarlane)

The ERRORR module of the NJOY system produces processed multigroup variance-covariance matrices, as well as processed multigroup cross sections, from ENDF/B input. The COVR module of NJOY reads the multigroup data output by ERRORR and produces standard plots of relative standard deviation and gray-shaded graphic representations of the correlation matrices. At least for some cases, this representation is more helpful than the products of alternative plotting packages. However, COVR does require the availability of the DISSPLA proprietary plotting software package. The new NJOY User's Manual<sup>4</sup> includes code description, operating instructions, etc., for both the ERRORR and COVR modules.

ERRORR is a flexible program that allows the user several choices in the particular method used to calculate covariances. The first method, the "point-wise" approach, is used when one has access to a data set containing resonance-reconstructed and linearized cross sections in the NJOY "point-ENDF," or PENDF format. The user can produce such a data set using the RECONR and BROADR modules of NJOY. For example, a PENDF tape containing all of the reactions on the ENDF/B-V dosimetry file, with all resonances reconstructed and Doppler broadened to 300 K, has been produced recently at Los Alamos and is available from the Los Alamos Nuclear Data Group. In order to keep the size of this data file down to a manageable size (56 000 card images), a relatively coarse accuracy criterion (1% for non-fissile nuclides, 5% for fissiles) was employed in the resonance-reconstruction calculation.

In this mode of operation, the user can specify a group structure with complete flexibility (up to 620 user groups are allowed). The ERRORR module will determine the union of the user's energy grid and the ENDF/B evaluator's grid for the material of interest. The relationship between these three grids is illustrated in Fig. 27.

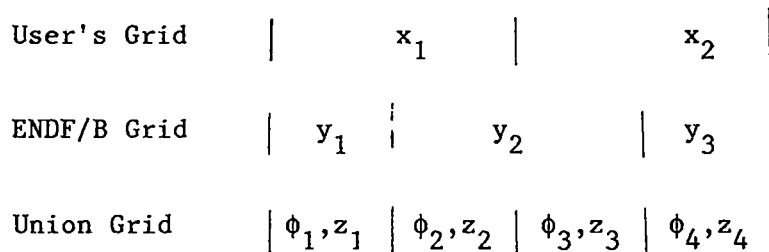


Fig. 27. Illustration of energy grid relations.

After forming the union grid, ERRORR integrates  $\sigma(E)$  and the user-supplied weight function  $\phi(E)$  to obtain the cross sections  $z_k$  and "fluxes"  $\phi_k$ , multi-grouped on the union grid. These, in turn, are used to calculate multigroup cross sections  $x_i$  on the user's grid according to

$$x_i = \frac{\sum_{k \in i} \phi_k z_k}{\sum_{k \in i} \phi_k} . \quad (1)$$

In order to calculate the covariances of  $x_i$ , the methodology of ERRORR assumes that the  $\phi(E)$  is free of uncertainty, so that the "propagation-of-errors" formula can be used,

$$\text{cov}(x_i, x_j) = \sum_{\substack{k \in i \\ \ell \in j}} a_{ik} a_{j\ell} \text{cov}(z_k, z_\ell) , \quad (2)$$

where the "sensitivity coefficients"  $a_{ik}$  are the normalized group fluxes,

$$a_{ik} = \frac{\phi_k}{\sum_{k \in i} \phi_k} . \quad (3)$$

The union-grid covariances  $\text{cov}(z_k, z_\ell)$  in Eq. (2) are formed from the numerical data in the ENDF/B covariance files by combining them, in the ENDF/B prescribed manner,<sup>56,57</sup> with the union-grid cross sections  $z_k$ .

The final step, if the user requests it, is to convert the absolute covariances, Eq. (2), to relative covariances,

$$\text{relcov}(x_i, x_j) = \frac{\text{cov}(x_i, x_j)}{x_i x_j} . \quad (4)$$

A slightly different calculational path is followed if one wishes to start from a multigroup cross-section library rather than pointwise data. ERRORR will accept such multigroup cross-section input, but only in the format produced by the NJOY group-averaging module GROUPR. Such a library contains both multigroup cross sections and group integrals of the weight function used to produce the cross sections.

In the multigroup input mode, the required union-grid cross sections and fluxes are obtained by collapsing (or expanding) the cross sections and fluxes on the input library. At present, no provision is made for replacing the library group fluxes with a set more appropriate for a given application. If a "library" group is subdivided by a union-group boundary, ERRORR assumes the cross section and weighting function are both energy-independent, in order to estimate  $\phi_k$  and  $z_k$  above and below the point of subdivision. The remainder of the calculation proceeds as with pointwise input.

A 620-group (SAND-II) GROUPR output library has been produced recently for the ENDF/B-V dosimetry materials, using a constant weight function. This library is also available on request, either in the GROUPR output format, or as a PENDF tape. With the latter, the ERRORR calculations can be performed in the "pointwise" mode, thus avoiding the library-group-flux problem mentioned above.

In some materials, and in certain energy regions, the cross-section uncertainty is dominated by the uncertainty in resolved resonance parameters. One noteworthy example is  $^{63}\text{Cu}(n,\gamma)^{64}\text{Cu}$  (ENDF/B-V Material 6435) in the energy range from 10 eV to 15.9 keV, where the entire cross-section uncertainty is represented by means of resonance-parameter uncertainties. The same is true of  $^{237}\text{Np}(n,f)$  (ENDF/B-V Material 6337) from 0 to 10 eV.

Beginning with the (10/81) version of ERRORR, the resonance-parameter contribution to the uncertainty in infinite-dilution fission and capture cross sections is included automatically when cross-section covariances are processed.

This contribution is obtained from the Breit-Wigner formula for the fission and capture areas of a resonance,  $A_f$  and  $A_\gamma$ , respectively. By differentiating this formula with respect to the resonance parameters, one obtains a set of sensitivities. With these sensitivities and the covariance matrix of the parameters from ENDF/B, one can apply a propagation-of-errors formula, similar to Eq. (2), to obtain the covariances  $\text{cov}(A_\gamma, A_\gamma)$ ,  $\text{cov}(A_\gamma, A_f)$ , and  $\text{cov}(A_f, A_f)$ . These results then are added to the ENDF-specified "long-range" cross-section covariances.

The resonance contribution is properly weighted with the isotopic abundance and the ratio of the weight function at the resonance to the average weight in the group. It is assumed, however, that the area of a resonance lies entirely within the group that contains the resonance energy  $E_r$ . Because of this assumption, and because ENDF/B provides no correlations between parameters of different resonances, the calculated resonance-parameter contribution affects only the diagonal elements of the affected matrices.

With the implementation of this feature, the uncertainty in the capture cross section of  $^{63}\text{Cu}$ , for example, computed for a group that contains the large 577-eV resonance is 3.0%, rather than zero, as in earlier ERRORR versions.

The (10/81) version of ERRORR also handles explicit cross-material covariances. The only explicit cross-material covariances appearing in ENDF/B-V pertain to fission  $\bar{\nu}$  values, but there is a clear need for more information of this type in future versions of ENDF/B.

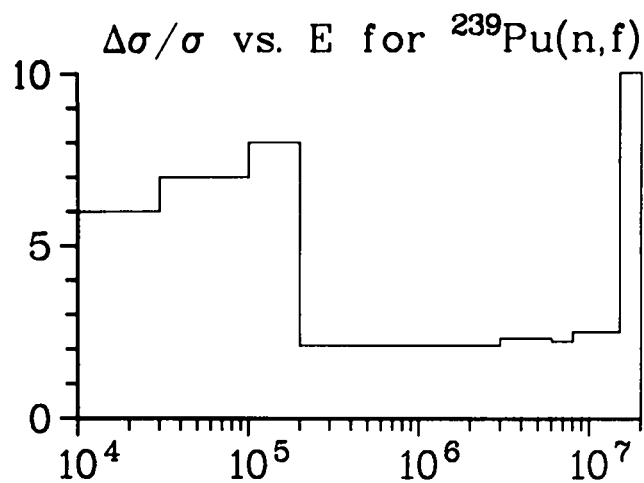
A third, more recent, extension of the program allows the processing of covariances in cases when one cross section is measured relative to a well-known "standard" cross section. In such a case, the evaluator may represent the uncertainty in the first cross section as being the sum of two components. The first component is described by an explicit statement of the uncertainty in the measured ratio, whereas the second component, due to uncertainty in the standard, is represented implicitly, with the details provided only in the ENDF/B evaluation for the standard reaction.

In the ENDF/B-V dosimetry file, this situation occurs for the  $^{238}\text{U}(n,\gamma)$  reaction (ENDF/B Material 6398), which was measured relative to  $^{10}\text{B}(n,\alpha)$  from 4 keV to 20 keV, and the  $^{239}\text{Pu}(n,f)$  reaction (ENDF/B Material 6399), which was measured relative to  $^{235}\text{U}(n,f)$  from 0.2 to 15 MeV. When ERRORR was modified to include the uncertainty in the standard, there was little effect for  $^{238}\text{U}(n,\gamma)$ ,

but there was a noticeable increase in the uncertainty of  $^{239}\text{Pu}(n,f)$ , from about 2% to 4-5% in the MeV region. The energy-to-energy correlation matrix is also affected, as can be seen by comparing Fig. 28 with Fig. 29. This ratio-to-standard capability is not implemented in the (10/81) version of ERRORR, but a set of code changes to accomplish this is available from the authors on request.

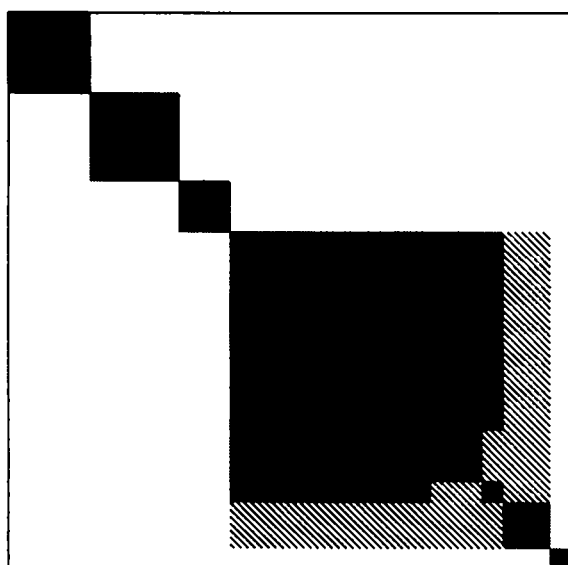
Another recent extension [also not included in the (10/81) version] allows the processing of the "lumped-partial" covariance format approved by the Cross-Section Evaluation Working Group in May 1981. This format allows the evaluator to specify a group of nuclear reactions and to give the uncertainty only in the sum of the cross sections for those reactions. One can, for example, replace 30 or 40 discrete-level inelastic cross sections with 5 or 6 "lumped" cross sections when constructing the covariance files. Since the volume of the covariance data varies, in general, as the square of the number of reactions, this lumping can greatly reduce the size of the files.

The first ENDF/B evaluation to employ the lumped-partial format is P. G. Young's evaluation<sup>58</sup> for  $^7\text{Li}$  (ENDF/B-V, Rev. 2). All covariance data for this evaluation have been successfully processed into multigroup form using ERRORR. The covariances for MT 854 (a single "real" level with an excitation energy of 4.63 MeV) with MT 855 (5 lumped pseudo-levels,<sup>59</sup> with excitation energies ranging from 4.75 MeV to 6.75 MeV) have been plotted using COVR in Fig. 30. The large negative correlations along the diagonal result from the fact that, below 10 MeV, these inelastic reactions are the major contributors to the fairly well-known tritium-production cross section. An upward variation in one reaction at a given energy must be accompanied by a downward change in the other. As shown in the plot, the magnitude of this negative correlation diminishes at higher energies, as other reactions begin to contribute significantly to the tritium-production cross section. Plots of this type, prepared using ERRORR and COVR, have proven to be useful tools in the validation of the covariance files of new evaluations.

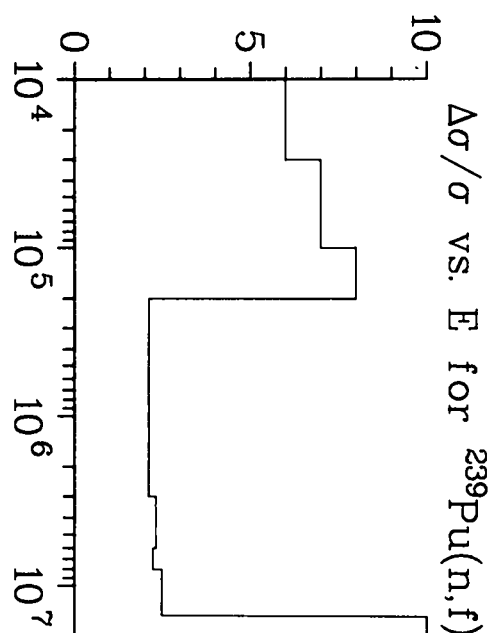


Linear Axes:  
Rel. Standard  
Deviation (%)

Logarithmic Axes:  
Energy (eV)



Correlation Matrix



Key:

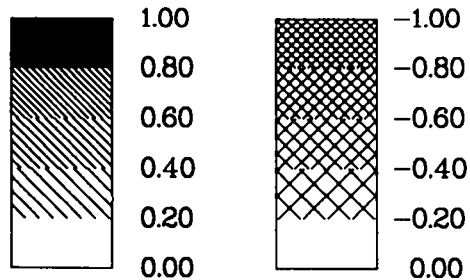


Fig. 28. Covariance data for  $^{239}\text{Pu}(n,f)$ , neglecting uncertainty in standard.

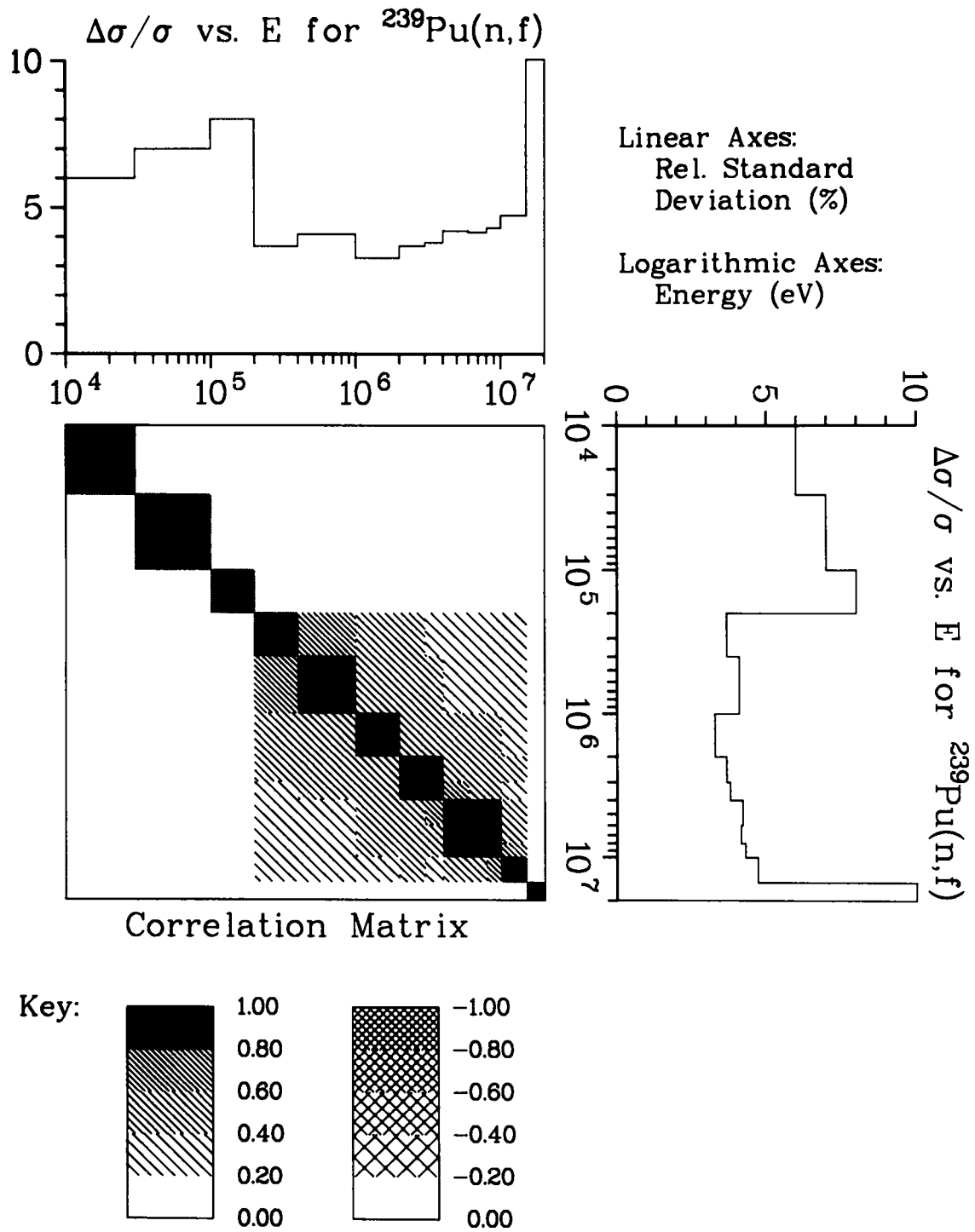
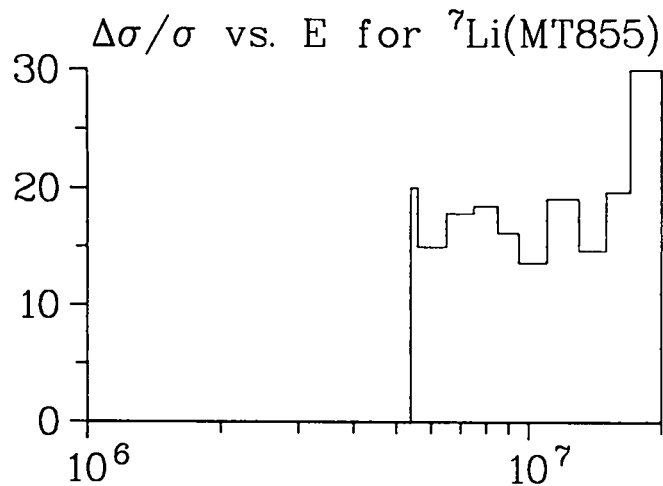
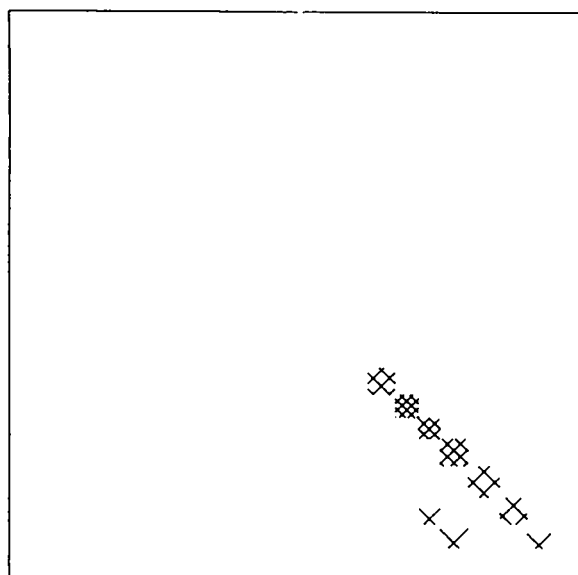


Fig. 29. Covariance data for  $^{239}\text{Pu}(n,f)$ , including uncertainty in standard.

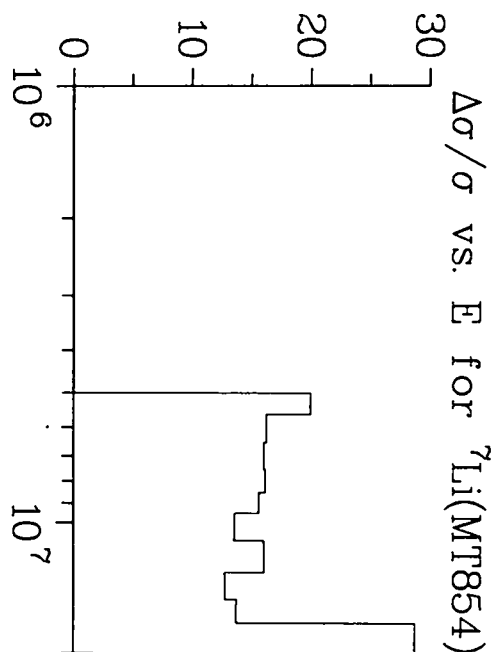


Linear Axes:  
Rel. Standard  
Deviation (%)

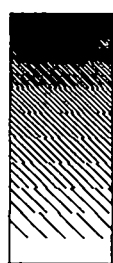
Logarithmic Axes:  
Energy (eV)



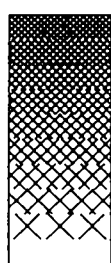
Correlation Matrix



Key:



1.00  
0.80  
0.60  
0.40  
0.20  
0.00



-1.00  
-0.80  
-0.60  
-0.40  
-0.20  
0.00

Fig. 30. Covariance data for  ${}^7\text{Li}(\text{MT854})$  with  ${}^7\text{Li}(\text{MT855})$ .